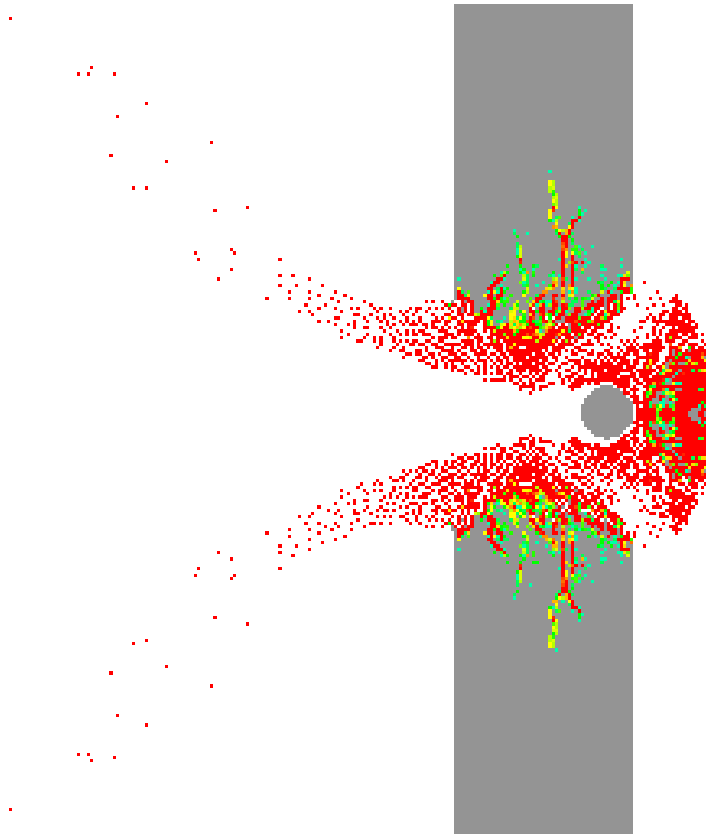


# CHALMERS



## Concrete Structures Subjected to Fragment Impacts

Dynamic Behaviour and Material Modelling

JOOSEF LEPPÄNEN

*Department of Structural Engineering and Mechanics*  
*Concrete Structures*  
CHALMERS UNIVERSITY OF TECHNOLOGY  
Göteborg, Sweden, 2004



THESIS FOR THE DEGREE OF DOCTOR OF PHILOSOPHY

# Concrete Structures Subjected to Fragment Impacts

Dynamic Behaviour and Material Modelling

JOOSEF LEPPÄNEN

Department of Structural Engineering and Mechanics  
Concrete Structures  
CHALMERS UNIVERSITY OF TECHNOLOGY  
Göteborg, Sweden, 2004

Concrete Structures Subjected to Fragment Impacts  
Dynamic Behaviour and Material Modelling  
JOOSEF LEPPÄNEN  
ISBN 91-7291-511-0

© JOOSEF LEPPÄNEN, 2004

Doktorsavhandlingar vid Chalmers tekniska högskola  
Ny serie nr. 2193

ISSN 0346-718x  
ISSN 1651-8357  
Publication 04:4  
Archive no. 31

Department of Structural Engineering and Mechanics  
Concrete Structures  
Chalmers University of Technology  
SE-412 96 Göteborg  
Sweden  
Telephone: + 46 (0)31-772 1000

Cover:  
Fragment impacting a concrete target; see Figure 5.8.

Chalmers Reproservice / Department of Structural Engineering and Mechanics  
Göteborg, Sweden, 2004

Concrete Structures Subjected to Fragment Impacts  
Dynamic Behaviour and Material Modelling  
JOOSEF LEPPÄNEN  
Department of Structural Engineering and Mechanics  
Concrete Structures  
Chalmers University of Technology

## ABSTRACT

As concrete is commonly used for protective structures, how a blast wave and fragment impacts from an explosion affect the concrete is an important issue. Concrete subjected to explosive loading responds very differently from statically loaded structures. The compressive and tensile strengths and the initial stiffness increase due to the strain rate effects. When fragments penetrate, spalling occur at the impact zone and scabbing may occur on the reverse side of a wall, or even perforation, with a risk of injury to people inside the structure.

The principal aim of this thesis is to improve the current knowledge of the behaviour of concrete structures subjected to blast and fragment impacts. The main focus is on numerical modelling of fragment impacts on plain concrete members. In addition, experiments in combination with numerical analyses were conducted to deepen the understanding of concrete subjected to blast wave and fragment impacts. In the experiments, both multiple and single fragments were shot at thick concrete blocks. To capture the response of the concrete material behaviour, both the fragment impacts and the blast wave must be taken into account. The damage in the spalling zone is caused by the fragment impacts, whereas the major stress wave that propagates is caused mainly by the blast wave.

To predict the penetration depth of the fragment impacts, spalling and scabbing in concrete with numerical methods, material models that take into account the strain rate effect, large deformations and triaxial stress states are required. The depth of penetration depends mainly on the compressive strength of the concrete. However, to model cracking, spalling and scabbing correctly in concrete, the tensile behaviour is very important. The RHT model in AUTODYN was used for the numerical analyses. The RHT model does not describe the concrete behaviour in tension accurately: the softening is linear and the strain rate dependency does not fit experimental results. Hence, a bi-linear softening law and a strain rate law were implemented in the model. By parametrical studies it was shown that the tensile strength, fracture energy and the strain rate law influenced the cracking and scabbing of concrete. By implementing the bi-linear softening law and a modified strain rate dependent law, the results of the numerical analyses were improved for projectile and fragment impacts on concrete.

Key words: concrete; fragment and projectile impacts; blast wave; numerical simulations; penetration; perforation; spalling; scabbing; dynamic loading; strain rate.

Splitterbelastade betongkonstruktioner  
Dynamiska egenskaper och materialmodellering  
JOOSEF LEPPÄNEN  
Institutionen för konstruktion och mekanik  
Betongbyggnad  
Chalmers tekniska högskola

## SAMMANFATTNING

Skyddsrum är oftast betongkonstruktioner. En viktig frågeställning är hur betongen påverkas av stötvåg- och splitterbelastning orsakad av en explosion. Betongkonstruktioner utsatta för explosionslaster där en stötvåg utbreder sig och splitter träffar konstruktionen uppför sig mycket annorlunda än konstruktioner som är utsatta för statisk belastning. Betongens tryck- och draghållfasthet och den initiella styvheten ökar på grund av ökad töjningshastighet. Betongen utsatt för denna typ av belastning erhåller kraftig sprickbildning och kratar uppstår när splittret träffar betongen. När splittret penetrerar betongen djupt, kan utstötning ske på motsatta sidan av anslaget, eller till och med genomträngning, med risk för skada att personer inuti byggnaden.

Målsättningen med avhandlingen är att öka kunskapen om betongkonstruktioner utsatta för stötvågs- och splitterbelastning. Arbetet har huvudsakligen varit inriktat på numerisk modellering av splitterbelastning. Dock har även experiment i kombination med numeriska analyser genomförts i detta arbete, där tjocka betongblock har skjutits med stötvåg- och splitterbelastning. För att fånga betongens respons vid stötvågs- och splitterbelastning i numeriska analyser är det nödvändigt att både splitter och stötvågen beaktas. Splittret orsakar avskalning på ytan medan spänningstången som propagerar är huvudsakligen orsakad av stötvågen.

För att kunna följa penetrationsförlopp i betong med numeriska metoder behövs materialmodeller där töjningshastighetsinverkan, stora deformationer och triaxiella spänningstillstånd kan beaktas. Inträngningsdjupet styrs huvudsakligen av betongens förmåga att motstå tryckkrafter. För att noggrant modellera sprickbildning, kraterbildning och utstötning i betong är betongens materialegenskaper vid drag mycket viktigt. RHT modellen i programmet AUTODYN har nyttjats för de numeriska beräkningarna. RHT modellen beskriver inte noggrant betongens materialegenskaper vid drag, då betongens mjuknande beskrivs med ett linjärt samband och töjningshastighets beroende i modellen följer inte experimentella resultat. För att öka noggrannheten i de numeriska analyserna för projektil- och splitterbelastning har ett bi-linjärt mjuknande och ett modifierat töjningshastighetsberoende implementerats i RHT modellen. Parameterstudier har visat att betongens draghållfasthet, brottenergi samt töjningshastighetsberoendet påverkar betongens sprickbildning och utstötning. För projektil- och splitterbelastning har noggrannheten ökat i de numeriska analyserna genom dessa implementeringar.

Nyckelord: betong; splitter; projektil; stötvåg; numerisk simulering; penetration; perforering; kraterbildning; utstötning; dynamisk belastning; töjningshastighet.

## LIST OF PUBLICATIONS

This thesis is based on the work contained in the following papers, referred to by Roman numerals in the text. For more than one author, the contributions of the authors to the work are given for each paper.

- I. Leppänen, J. and Gylltoft, K. (2003): Concrete Structures Subjected to Blast and Fragment Impacts. *Nordic Concrete Research*, 1/03, 2003, pp. 65-84.

Work done by Leppänen, J., supervised by Gylltoft, K.

- II. Leppänen, J. (2003): Numerical Simulation of Projectile Penetration in Concrete. *Nordic Concrete Research*, 2/03, 2003, pp. 84-103.

- III. Leppänen, J. (2004): Experiments and numerical analyses of blast and fragment impacts on concrete. Accepted for publication in the *International Journal of Impact Engineering*. Article in Press, 2004. 18 pp.

- IV. Leppänen, J. (2004): Concrete subjected to projectile and fragment impacts: Modelling of crack softening and strain rate dependency in tension. Submitted to *International Journal of Impact Engineering*, in September 2004. 14 pp.

## OTHER PUBLICATIONS BY THE AUTHOR

During the course of this work, subsequent results and some additional results have been presented on several occasions. These publications are:

## LICENTIATE THESIS

Leppänen, J. (2002): *Dynamic Behaviour of Concrete Structures subjected to Blast and Fragment Impacts*. Licentiate Thesis. Publication no. 02:2, Archive no. 31. Department of Structural Engineering, Chalmers University of Technology, Göteborg, Sweden, April 2002. 71 pp.

## CONFERENCE PAPERS

Leppänen, J. (2004): Fragment impacts into concrete, *Eighth International Conference on Structures Under Shock and Impact*, Crete, Greece, March 2004, pp. 63-71.

Leppänen, J. and Gylltoft, K. (2002a): Numerical Simulation of Concrete Penetration with a Steel Projectile, *XVIII Nordic Concrete Research Symposium*, Helsingör, Denmark, June 2002, pp. 273-275.

Leppänen, J. and Gylltoft, K. (2002b): Finite element analyses of concrete penetration with a steel projectile. Comparison of Lagrangian and Eulerian techniques, *Seventh International Conference on Structures Under Shock and Impact*, Montreal, Canada, May 2002, pp. 59-68.

## REPORTS AND OTHER PUBLICATIONS

Leppänen, J. (2003): *Splitterbelastad betong - Experiment och numeriska analyser* (Fragment impacts into concrete - Experiments and numerical analyses, In Swedish). Report no. 03:6, Department of Structural Engineering and Mechanics, Concrete Structures, Chalmers University of Technology, Göteborg, Sweden, August 2003, 80 pp.

Leppänen, J., Ekengren, B., Gylltoft, K., Johansson, M. and Plos, M. (2002): Explosionsbelastade betongkonstruktioner (Concrete Structures subjected to Explosions, In Swedish), *Bygg & teknik*, Vol. 7, No. 02, Stockholm, Sweden, October 2002, pp. 54-59.

Leppänen, J. (2001): *Finita Elementanalyser av splitterbelastade betongkonstruktioner - Inledande studie med ABAQUS/Explicit* (Finite Element analyses of concrete structures subjected to fragment impacts - Preliminary study by ABAQUS/Explicit, In Swedish). Report no. 01:1, Department of Structural Engineering, Concrete Structures, Chalmers University of Technology, Göteborg, Sweden, March 2001, 72 pp.



# Contents

ABSTRACT	I
SAMMANFATTNING	II
LIST OF PUBLICATIONS	III
PREFACE	VII
NOTATIONS	VIII
1 INTRODUCTION	1
1.1 Background	1
1.2 Aim, scope and limitations	1
1.3 Outline of the thesis	2
1.4 Original features	2
2 DYNAMIC LOADING OF CONCRETE STRUCTURES	3
2.1 Blast waves	3
2.2 Fragment impacts	5
2.3 The behaviour of concrete under static loading	11
2.4 The behaviour of concrete under high lateral pressure	12
2.5 Strain rate effects for concrete under uniaxial loading	14
3 EXPERIMENTS ON FRAGMENT IMPACTS INTO CONCRETE	17
3.1 Introduction	17
3.2 Concrete blocks that have been shot	17
3.3 Uniaxial compressive and tensile tests	18
3.4 Thin-ground sections	21
4 NUMERICAL MODELLING	25
4.1 Numerical techniques	25
4.2 The equation of state, <i>EOS</i>	26
4.3 The RHT model for concrete	28
4.4 Mesh dependency	31
5 THE IMPROVED MATERIAL MODEL	33
5.1 General background	33
5.2 The modified crack softening law	33
5.3 The modified strain rate law for concrete in tension	34

5.4	Mesh dependency	37
5.5	Results with the improved material model	39
6	CONCLUSIONS	42
6.1	General conclusions	42
6.2	Suggestions for future research	43
7	REFERENCES	45

APPENDIX A      Empirical equations

APPENDIX B      Equations to determine the dynamic increase factor

APPENDIX C      Input data for modelling concrete

PAPER I - PAPER IV

# Preface

The present study treats concrete structures subjected to fragment impacts. The work presented in this thesis was carried out from February 2000 to October 2004 at the Department of Structural Engineering and Mechanics, Concrete Structures, Chalmers University of Technology, Sweden. Financial support for this work was provided by the Swedish Rescue Services Agency.

I would like to express gratitude to my supervisor, Professor Kent Gylltoft, for his valuable guidance and support during these years. I am also grateful to the reference group members of the project, “Dynamic behaviour of concrete structures subjected to blast and fragment impacts”. The members are Björn Ekengren, from the Swedish Rescue Services Agency, Mario Plos, from Chalmers, and Morgan Johansson from Reinertsen AB. These people, together with Kent Gylltoft and myself, have met for this project several times per year. The meetings have been creative and balanced well by humour, with fruitful and lively discussions of the project and its progress. Additional thanks go to Morgan for proof reading and offering valuable comments on all my papers and this thesis.

Furthermore, I would like to thank Lars Wahlström for the great work in the laboratory during the experimental part of this project. Thanks go also to the staff at Swedish defence research agency, FOI for the help with the experiments. I would also like to thank the staff at Century Dynamics and Leo Laine for the support with the program AUTODYN.

Finally, I thank my present and former colleagues for their support and interesting discussions on material modelling and the general behaviour of concrete during our concrete group days, doctoral meetings and coffee breaks, particularly Peter Grassl, Ingemar Löfgren and Mathias Johansson.

Göteborg, October 2004

Joosef Leppänen

# Notations

## Upper case letters

$A$	Area, parameter for compressive yield surface
$B$	Parameter for residual yield surface
$D$	Damage
$E$	Young's modulus
$G_F$	Fracture energy
$K$	Bulk modulus
$M$	Parameter for residual yield surface
$N$	Parameter for compressive yield surface
$M_h$	Weight of the bomb case
$P_s^+, P_s^-$	Peak pressures
$Q$	Charge weight
$T^+, T^-$	Positive time duration, negative time duration
$U_s$	Shock velocity
$V, V_0$	Volume, Initial volume
$V_s$	Striking velocity
$Y, Y^*$	Yield strength, yield strength normalized by compressive strength
$Y_{TXC}$	Pressure dependent yield strength
$Y_{residual}^*$	Residual strength

## Lower case letters

$b$	Constant to describe pressure–time history
$d_{pf}$	Thickness to prevent perforation
$e$	Specific internal energy
$f_c$	Compressive strength
$f_t$	Tensile strength
$f_{ts}$	Static tensile strength
$k, k_1, k_2$	Crack softening slopes
$l$	Length
$i^+, i^-$	Positive impulse, negative impulse
$m_f$	Fragment mass
$p, p^*$	Pressure, pressure normalized by compressive strength

$p_{crush}$	Initial compaction pressure
$p_0$	Atmospheric pressure
$r, r_0$	Radius, Initial radius
$t$	Time
$v_i$	Initial fragment velocity
$v_r$	Fragment velocity after a distance, r
$w$	Crack opening
$w_u$	Ultimate crack opening
$x$	Depth of penetration

### Greek letters

$\alpha$	Strain rate factor
$\delta$	Strain rate factor
$\varepsilon$	Strain
$\varepsilon_c$	Concrete strain
$\varepsilon_u$	Ultimate concrete strain in tension
$\dot{\varepsilon}$	Strain rate
$\dot{\varepsilon}_0, \dot{\varepsilon}_s$	Static strain rate
$\mu$	Compression
$\nu$	Poisson's ratio
$\rho$	Density
$\rho_0, \rho_s$	Initial density, solid density
$\sigma$	Stress
$\sigma_1, \sigma_2, \sigma_3$	Principal stresses
$\sigma_c$	Concrete stress
$\sigma_{lat}$	Lateral stress



# 1 INTRODUCTION

## 1.1 Background

The terrorist attack on 11<sup>th</sup> September 2001 shocked the world. The risk of terrorist attacks may not be as high in Sweden as in other parts of the world. However, the wise are prepared for the unknown future; it is important to have tools to analyse loading phenomena such as concrete structures subjected to explosive loading. Since massive concrete structures withstand blast waves and fragment impacts effectively, they are often used for protection. According to the Swedish Shelter Regulations, Ekengren (2003), a shelter should withstand, "...the effect of a pressure wave corresponding to that produced by a 250-kilogram GP (General Purpose) bomb with 50% by weight TNT that bursts freely outside at a distance of 5.0 metres from the outside of the shelter during free pressure release": Henceforth, this is referred to as the design bomb. Furthermore, according to these regulations, the shelter shall withstand the effect of fragment impacts from the design bomb. Normally, the thickness of concrete is designed to withstand the fragment impacts, while and a static load, with a dynamic increase factor, approximates the blast load.

Chalmers University of Technology has been collaborating with the Swedish Rescue Services Agency for many years, to study the behaviour of concrete structures subjected to blast and fragment impacts; see Plos (1995), Johansson (2000), Leppänen (2002), Leppänen *et al.* (2002) or Rempling (2004).

A blast load is characterized by its short duration. By computations, Johansson (2000) showed how a shelter subjected to a blast wave responded at the most critical stage, i.e. the first few milliseconds. If the load was applied fast enough, some parts of the structure were not affected by the loading, while other parts of it had already failed. In addition to the blast wave, the detonation of a General Purpose (GP) bomb causes fragments to fly against the civil defence shelter. This thesis includes the effects of fragment impacts in the numerical analyses. To examine what happens when a fragment strikes a concrete structure, there are several factors that must be taken into account. These include fragment impacts and damage mechanisms in concrete, as well as the dynamic behaviour of concrete under high pressures.

## 1.2 Aim, scope and limitations

The principal aim of the research project, dynamic behaviour of concrete structures subjected to blast and fragment impacts, is to improve the current knowledge of the behaviour of concrete structures subjected to blast and fragment impacts. This thesis focuses mainly on studies of projectiles and fragment impacts into plain concrete. The project goals include an understanding of the phenomena for concrete subjected to dynamic loading. Another aim was to improve the modelling of fragment impacts in plain concrete.

Experiments and numerical analyses were conducted for combined blast wave and fragment impacts in concrete. In both the experiments and analyses, the fragments were simplified as spherical ones. However, in real bomb detonation, the flying

fragments are not spherical; this limitation was chosen, however, to have as clear initial conditions as possible, both for the experiments and the numerical analyses.

Concrete structures are normally reinforced. In this thesis, the experiments and numerical analyses are limited to plain concrete (or slightly reinforced concrete members), such as blocks, cylinders or walls, as a starting point for examining and extending the knowledge of penetration, perforation, spalling, scabbing and cracking phenomena.

### **1.3 Outline of the thesis**

The thesis consists of an introductory part and four papers. The introductory part gives a background to the subjects treated in the papers and links them together. Although the main work is given in the papers, some new results are also presented in the first part.

- Chapter 2 gives general information on blast waves, fragment impacts and the dynamic behaviour of concrete.
- In Chapter 3, experiments on fragment impacts are discussed.
- Chapter 4 deals with numerical modelling.
- Chapter 5 explains the improved material model and shows some results.
- In Chapter 6 major conclusions are drawn and some suggestions for future research.
- Appendixes A, B and C, followed by Papers I to IV complete the thesis.

### **1.4 Original features**

The work presented in this thesis is a study of the behaviour of plain concrete subjected to blast and fragment impacts. It is shown that, by combining both experiments and numerical analyses, which form a powerful tool for deeper understanding of phenomena, fragment impacts can be modelled accurately by numerical methods. It is believed that the experiments done during this work are unique. Furthermore, by combined literature studies and numerical analyses, it was found that the strain rate law and the linear crack softening law must be improved in the software used in the numerical analyses. A modified strain rate law for tension and the bi-linear crack softening law, proposed by Gylltoft (1983), are implemented in the software AUTODYN (2004). It is believed that this implementation is the first. Thus, the contribution of this thesis meets the need for greater practical and deeper theoretical understanding of concrete structures subjected to blast and fragment impacts of the next generation of analysts.



## 2 DYNAMIC LOADING OF CONCRETE STRUCTURES

### 2.1 Blast waves

To understand the behaviour of concrete structures subjected to severe loading from military weapons, the nature and physics of explosions and the formation of a blast wave and reflections from a bomb must be comprehended. When the blast wave hits a concrete surface, a stress wave propagates through the concrete.

A shock wave resulting from an explosive detonation in free air is termed an air-blast shock wave, or simply a blast wave, see Baker (1973). The blast environment differs according to where the explosion takes place. In an airburst, a blast wave that hits the ground surface is reflected. The reflected wave coalesces with the incident wave, forming a Mach front, as shown in Figure 2.1. The point at which the three shock fronts meet – incident wave, reflected wave and the Mach front – is termed the triple point; blast wave reflections are further discussed in Paper I and in Baker (1973).

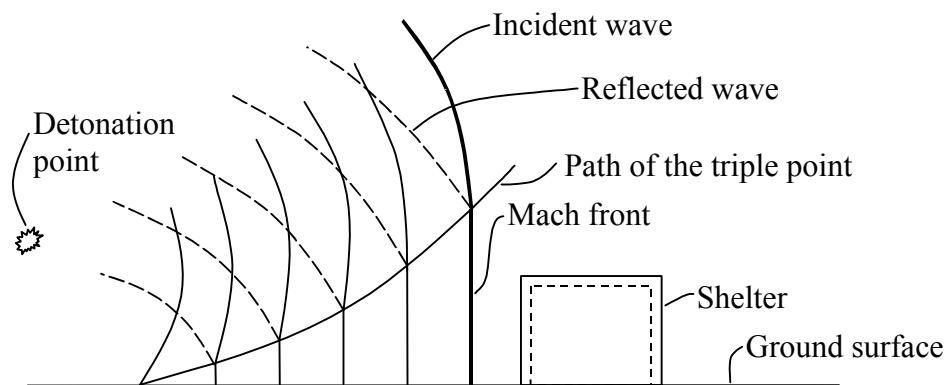


Figure 2.1 Blast environment from an airburst, based on Krauthammer (2000).

When there is a surface burst, the reflection occurs instantaneously from the ground surface, which generates a shock wave; this is termed a ground-reflected wave, as shown in Figure 2.2. At a relatively short distance from the burst, the wave front can be approximated by a plane wave.

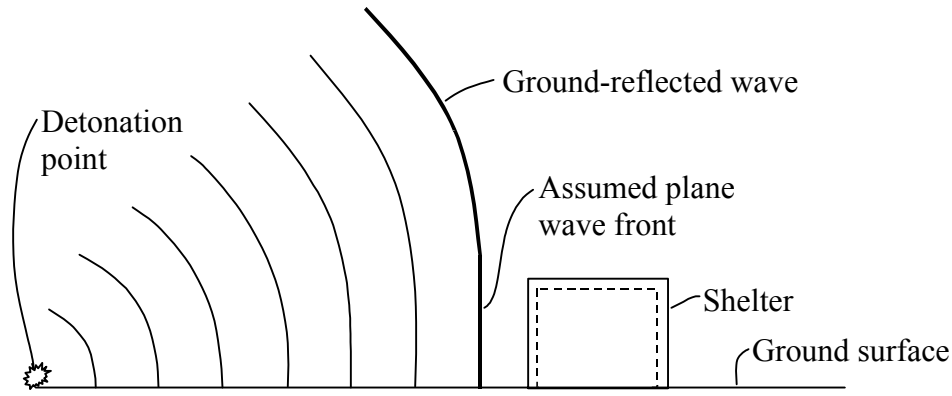


Figure 2.2 Surface burst blast environment, based on Krauthammer (2000).

The pressure-time history of a blast wave can be illustrated with an ideal curve as shown in Figure 2.3. The illustration is an idealization of an explosion. The pressure-time history is divided into positive and negative phases. In the positive phase, maximum overpressure,  $p_0 + P_s^+$ , rises instantaneously and then decays to atmospheric pressure,  $p_0$ , with time,  $T^+$ . The positive impulse,  $i^+$ , is the area under the positive phase of the pressure-time curve. For the negative phase, the maximum negative pressure,  $p_0 - P_s^-$ , has a much lower amplitude than the maximum overpressure. The duration of the negative phase,  $T^-$ , is much longer than that of the positive one. The negative impulse,  $i^-$ , is the area below the negative phase of the pressure-time curve. The positive phase is more interesting in studies of blast wave effects on concrete buildings because of the high amplitude of its overpressure and the concentration of the impulse.

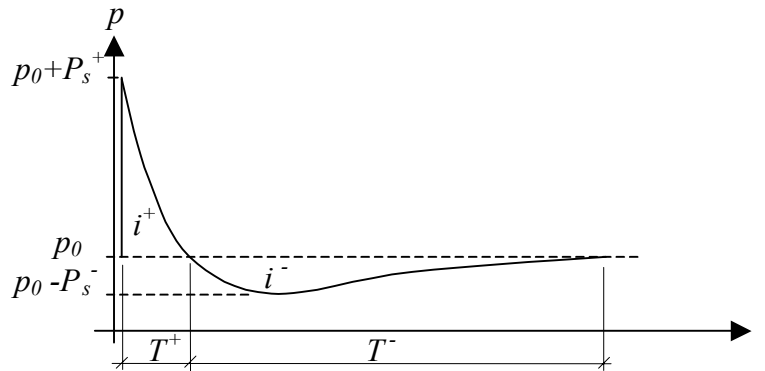


Figure 2.3 Pressure-time history from a blast.

The following exponential form expresses the positive phase of the pressure-time history in Figure 2.3, first noted by Friedlander (1939), according to Bulson (1997):

$$p(t) = p_0 + P_s^+ \left(1 - \frac{t}{T^+}\right) e^{-bt/T^+} \quad (2.1)$$

where  $p(t)$  is the overpressure at time  $t$  and  $T^+$  (the positive duration) is the time for the pressure to return to the atmospheric level,  $p_0$ . By selecting a value for the constant,  $b$  various pressure-time histories can be described. The peak pressure,

$p_0 + P_s^+$ , depends mainly on the distance from the charge and the weight of the explosives. In addition, if the peak pressure, the positive impulse and the positive time duration are known, the constant,  $b$ , can be calculated, and then the pressure-time history can be obtained.

Equation (2.1) is often simplified with a triangular pressure-time curve; see Bulson (1997)

$$p(t) = p_0 + P_s^+ \left(1 - \frac{t}{T^+}\right). \quad (2.2)$$

A detonation inside a building causes more damage than one outside the building, see Forsén (1989). The reason for this is that, in addition to the short duration of a blast wave, there is a long-duration wave, added by gas and heat, from the explosion, which cannot escape from the limited space. If the amplitude and the duration of the pressure are great enough, the walls and roof may be jerked apart. An important parameter for a building is the relationship between openings, known as the leakage area. With large leakage areas, the duration of the blast wave can be shortened and the damage possibly reduced.

## 2.2 Fragment impacts

When high explosives such as grenades, bombs, torpedoes, missiles or robots detonate, fragments fly out in all directions when the casing is broken. The fragments from the same kind of weapon can vary in size. The fragmentation process is discussed in Janzon (1978); and fragment data from different types of bombs can be found, for instance in Forsén and Sten (1994), Nordström (1995) or Andersson *et al.* (1989).

To explain the fragmentation process Janzon (1978) studied a cylinder. When an explosive detonates inside the cylinder, the cylinder expands and gets thinner. During the expansion, local radial tensile cracks develop from the outer surface inwards. However, the inner pressure caused by the shock wave from the detonation will delay or even stop the radial crack propagation; consequently, new radial cracks can be formed. This crack formation occurs simultaneously for the whole cylinder. When the radial crack formation is completed, shear cracks form from the inner surface. Again, this occurs simultaneously for the whole cylinder. The crack formations are completed when the shear cracks coincide with the radial cracks, which are schematically shown in Figure 2.4.

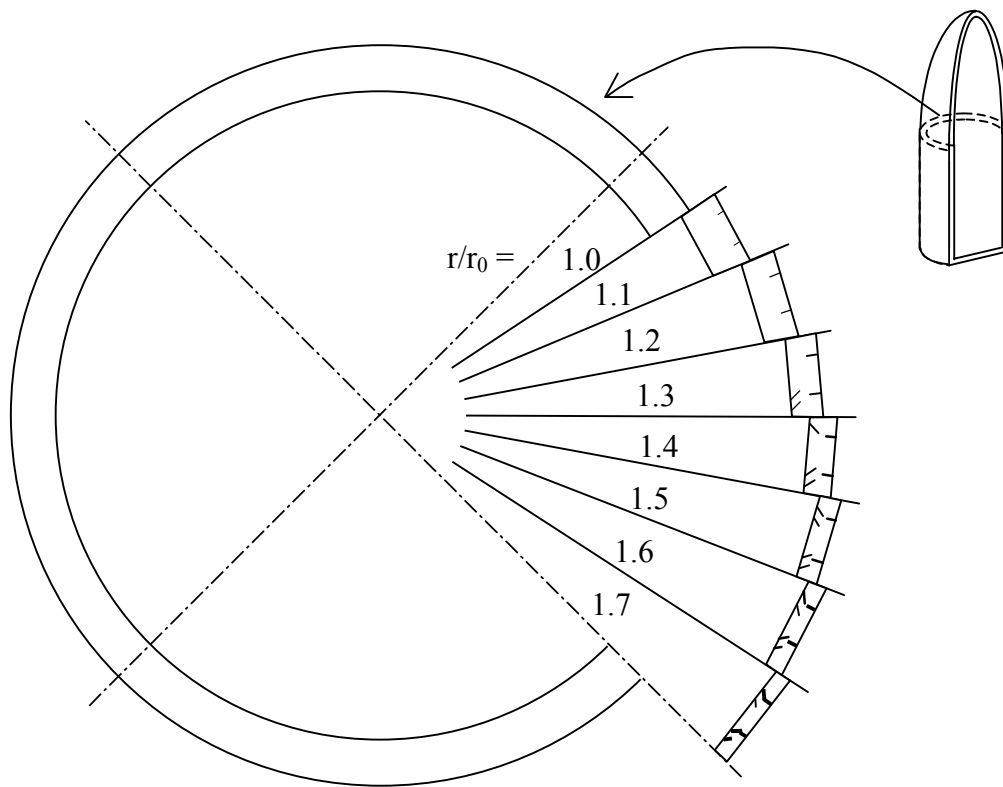


Figure 2.4 Schematic overview of the fragmentation process, plane view of the cross section from a bomb. Based on Janzon (1978).

The damage to concrete from fragment impacts depends on the properties of the fragments, i.e. the striking velocity, mass and area density [ $\text{kg/m}^2$ ]. Fragment impacts causes severe cracking and crushing in the concrete, which must be supported by reinforcement to prevent failure. When fragments strike a concrete structure, they penetrate into the concrete; the impact causes spalling at the point of contact and possible scabbing on the reverse side of the wall, see Figure 2.5. When 50 % penetration is reached, scabbing may become a problem according to Krauthammer (2000). Furthermore, the fragments can damage the reinforcement, and vibrations may reduce the bond between the concrete and reinforcement. When a stress wave propagates through the concrete and reaches the inside of a structure, it is reflected as a tensile wave; as concrete is weak in tension, this leads to scabbing on the inside. The amount of reinforcement is a highly critical parameter in regard to scabbing. Experiments show that the scabbing is reduced by increasing the amount of reinforcement since the reinforcement holds the concrete in place (the confinement effect), see Jonasson (1990).

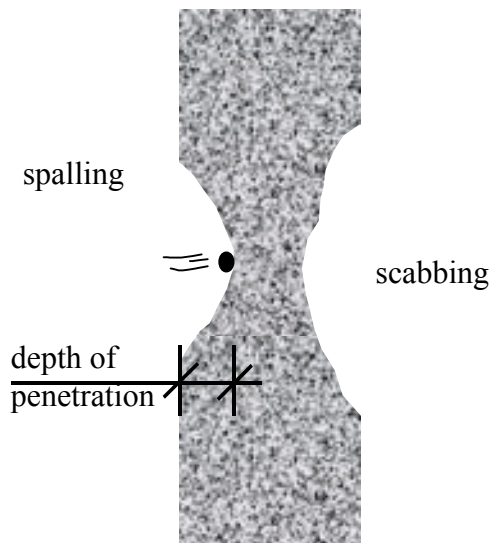


Figure 2.5 Definitions of depth of penetration, spalling and scabbing. Spalling takes place on the exposed side of the concrete wall and scabbing on the reverse side of the wall.

To estimate the fragment velocity, empirical formulas can be found in the literature, for example those proposed by von Essen (1973), Janzon (1978), Engberg and Karevik (1987), ConWep (1992) and Krauthammer (2000). The initial velocity of the fragments is determined by the amount of explosive material and size of the casing, which can be estimated with an equation. The fragment velocity is retarded in the air, in relation to the initial fragment velocity, the fragment mass and the type of fragment. Fragments from an explosion can fly through the air over very long distances, more than 1 000 m for heavy fragments, according to Engberg and Karevik (1987). For illustration, an example of fragment impacts is given with varying masses, as shown in Figure 2.6. As can be seen, the fragment velocity is highly dependent on the mass: for light fragments, the velocity is retarded faster than for heavy fragments. From the design bomb, see Section 1.1, the fragment weights are normally distributed from 1 to 50 grams, and the impact velocity varies approximately between 1 650 and 1 950 m/s. In Figure 2.6 the velocity for six fragment weights is shown, ranging from 5 to 400 grams; the equation can be found in Engberg and Karevik (1987) and in Appendix A.

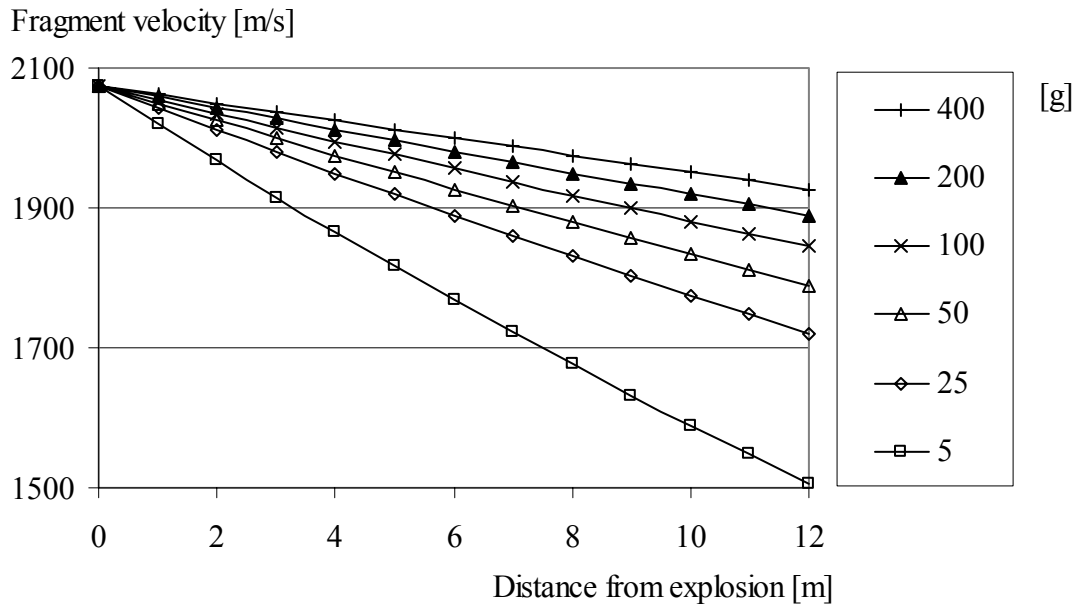


Figure 2.6 Fragment velocity from a design bomb, for fragment weights from 5 to 400 grams, based on equations from Engberg and Karevik (1987).

For comparison of different materials, the approximate depth of penetration is given by multiples of the depth of penetration for soft steel by using a factor; the factors are given in Table 2.1, taken from Engberg and Karevik (1987). By using a direct formula, from ConWep (1992), von Essen (1973) or Erkander and Pettersson (1985), the depth of penetration can be estimated for fragments penetrating concrete, as shown in Figure 2.7. The equations for these can be found in Appendix A. The assumptions in these formulations are not the same. The formulation in Erkander and Pettersson (1985) is a curve fit to their experimental results; it will not be discussed further here. In ConWep, the depth of penetration is a function of the fragment mass, the striking velocity and the concrete compressive strength. When using the equation from von Essen (1973) to estimate the depth of penetration, the concrete strength is not taken into account; the depth of penetration is a function of the fragment mass, and the striking velocity. Furthermore, the formulation in ConWep is designed to estimate penetration into massive concrete, while the von Essen one is for reinforced concrete. This may explain the divergence in estimations, such as the wide variation for heavy fragments in the high velocity impact region.

Figure 2.7 shows also experimental data from Erkander and Pettersson (1985) and Leppänen (2003); the data from Leppänen consists of both single and multiple fragment impacts. From these experimental data it can be seen that the formulation according to ConWep estimates the depth of penetration more accurately than the formulation in von Essen (1973).

Table 2.1 Penetration depth of common materials, taken from Engberg and Karevik (1987).

Material	Factor
Armour-plate	0.75
Soft steel	1.0
Aluminium	2
Reinforced fibre-glass plastic	4
Reinforced concrete	6
Pine wood	15
Sand	18
Water	50
Wet snow	70
Dry snow	140

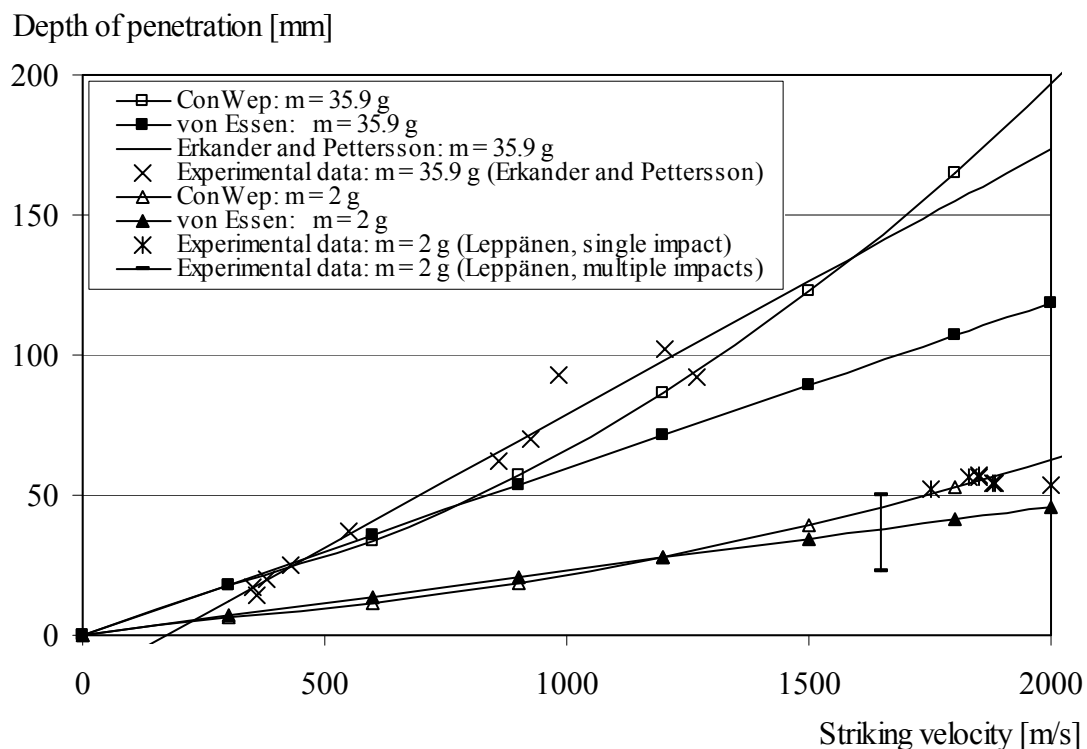


Figure 2.7 Comparison of empirical formulations of fragment impacts. ConWep (1992), von Essen (1973) and Erkander and Pettersson (1985); with experimental data from Erkander and Pettersson (1985) and Leppänen (2003).

The designer is interested of the thickness of the concrete wall that just prevents perforation. A rule of thumb is that when 70% penetration is obtained one may expect perforation, according to Krauthammer (2000). The thickness that prevents perforation can also be estimated by equations, see Krauthammer (2000) or Appendix A. For illustration, an example is given here: according to Swedish Rescue Services Agency shelter regulations, Ekengren (2003), a Swedish shelter above ground must have a minimum thickness of 350 mm. Table 2.2 shows the thickness required for a concrete wall that just prevents perforation by fragment weights from 5 to 400 grams with striking velocities up to 3 000 m/s. As shown, both the striking velocity and the mass are vital factors in the design of protective structures. The area marked grey indicates a thickness above 350 mm massive concrete (the required minimum thickness of a civil defence shelter above ground). For the normally distributed (1–50 grams) fragments from the design bomb, perforation would not be a problem, since the striking velocity for the 50 gram fragment is approximately 1 950 m/s. However, if single fragments of larges size than approximately 100 grams are released from the bomb, at a distance of 5 meters, perforation may occur.

Table 2.2 Thickness of concrete wall that just prevents perforation, compressive strength 30 MPa, for fragment weights from 5 to 400 grams with striking velocities up to 3 000 m/s, based on equations from Krauthammer (2000), see Appendix A.

Striking velocity [m/s]	Fragment mass [g]					
	5	25	50	100	200	400
300	22	39	50	65	84	108
600	30	54	70	91	118	153
900	39	74	97	127	167	220
1 200	53	101	134	177	235	312
1 500	70	135	180	239	318	424
1 800	90	175	233	312	416	556
2 100	112	220	295	394	528	707
2 400	138	271	363	487	653	877
2 700	166	327	439	590	792	1 064
3 000	196	389	522	702	943	1 268

A building is exposed not only to fragments or only a blast wave: the loading from a bomb is a combination of both the blast wave and flying fragments. Experiments show that a concrete building which is exposed to a combination of blast wave and fragments collapses more easily than one exposed only to a blast wave or to fragments, see Forsén and Edin (1991). Forsén (1997) showed that a 200 mm thick concrete plate collapsed when a combination of blast load and fragment impacts from



a distance of 14 m was applied; however, a similar concrete plate could withstand the same blast load at a distance of 5 m without fragment impacts.

The load from a detonation can be separated into a blast wave and a fragment impacts. Depending on the charge and the distance between the bomb and the target, the fragments may strike the concrete surface before, at the same time as, or after the blast wave. Figure 2.8 shows an example of the design bomb to compare the arrival time of the blast wave calculated according to ConWep (1992) and the arrival time of the fragments; for equations see Appendix A. For this type of bomb, the arrival times for the blast and the fragments coincide at a distance of approximately 5 m; at a greater distance, the fragments strike the target before the blast wave.

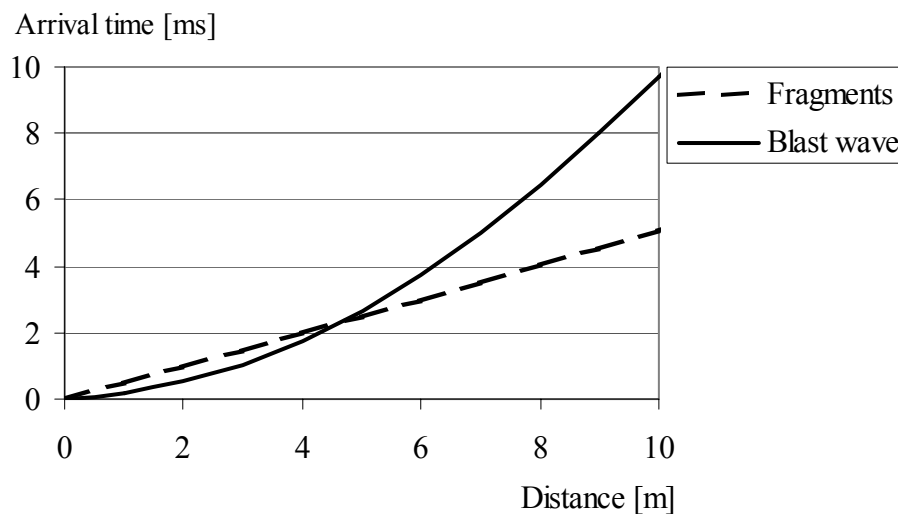


Figure 2.8 Calculated arrival time for a blast wave and fragments from the design bomb.

The difference in arrival time for a blast and fragments is less important for short distances, according to Forsén and Nordström (1992). This is so because the response time of a reinforced concrete wall is usually much longer than the difference between the arrival times of a blast and the fragments. The fragments would damage the wall before it is deformed. A very good estimation of the deflection can be made by simply superposing the impulse of the fragment impacts on the positive impulse of the blast wave, at the maximum blast pressure. Then the impulse can be simplified and estimated by using a triangular shape; the resistance of the wall can be assumed to be reduced by the fragments that comprise the very beginning of the load, see Forsén and Nordström (1992).

## 2.3 The behaviour of concrete under static loading

Concrete is often characterized by the uniaxial stress-strain relationship, as shown in Figure 2.9. Concrete is weak in tension: for normal-strength concrete, the ultimate tensile strength is less than one tenth of the ultimate compressive strength. Moreover, concrete is very brittle in tension: the softening phase is very steep when the peak-load has reached. The post-peak behaviour is normally characterised by the fracture energy,  $G_F$ . However, real structures are subjected to multiaxial stresses.

Richart *et al.* (1928) observed that confined concrete has greater strength and stiffness, and furthermore, strains are extended. In Figure 2.10, the stress-strain relationship for concrete in compression is shown for increasing lateral pressure (confined concrete).

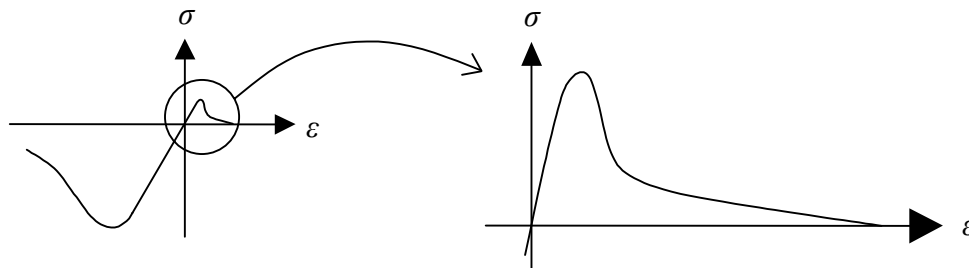


Figure 2.9 Schematic view of stress-strain relationship under uniaxial loading for concrete.

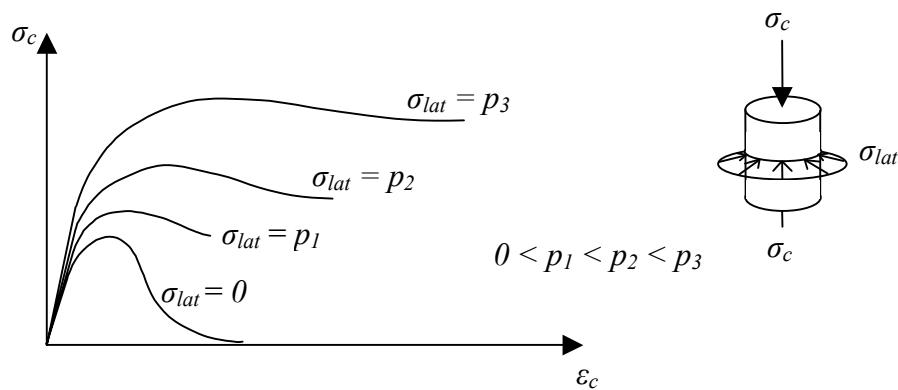


Figure 2.10 Schematic view of stress-strain relationship for rising lateral pressure in compressed concrete. Based on research by Richart *et al.* (1928).

## 2.4 The behaviour of concrete under high lateral pressure

When concrete is subjected to extremely high pressures, as in an impact situation, the lateral pressure suddenly becomes much higher. During fragment impacts, concrete is exposed to enormous confining pressures and behaves plastically, dissipating a large amount of energy. In addition, civil defence shelters have heavy reinforcement, which provides further confinement effects. The confining pressure in impact loading can be several hundred MPa. In a standard static triaxial test, the ultimate strength of concrete can increase greatly. Experiments by Bažant *et al.* (1996), with a uniaxial compressive strength of 46 MPa, showed that the ultimate strength increased up to 800 MPa, and the strains were extended as shown in Figure 2.11.

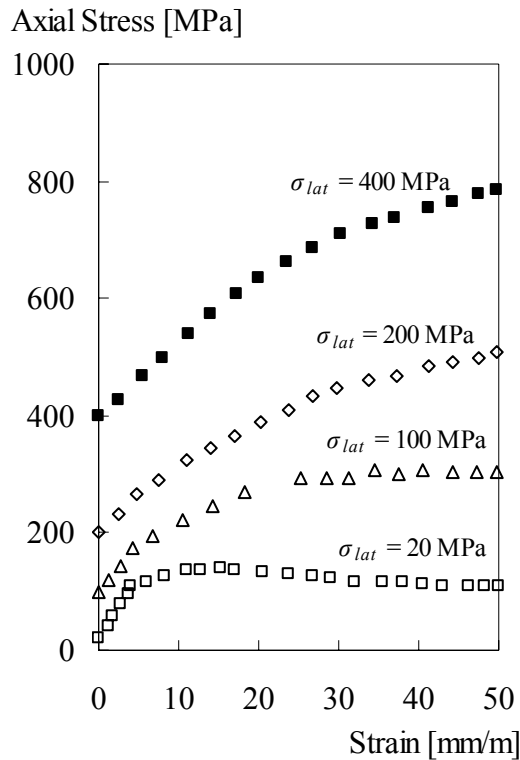


Figure 2.11 Stress-strain relationship for concrete at high lateral pressures, based on triaxial compression test data from Bažant *et al.* (1996). Uniaxial compressive strength 46 MPa.

Another characteristic of concrete behaviour is that it is not linear for hydrostatic pressure (mean value of the principal stress components); this can be illustrated by the relationship between hydrostatic pressure and density. However, for low-pressure levels the relationship is linear (elastic loading); with further loading, at a certain pressure level, micro cracking occurs in concrete, and the relationship becomes non-linear. Since concrete is porous, the pores collapse and the material is compacted. At a very high-pressure level, all of the pores are collapsed, and the relationship between hydrostatic pressure and density becomes linear again. The equation of state (*EOS*) relates the pressure to the local density and the local specific internal energy. In Figure 2.12 the *EOS* is illustrated for concrete. The initial density is designated  $\rho_0$  and the solid density is  $\rho_s$  which is defined as the density at zero pressure of the fully compacted solid. The phase when the material is compacting is known as plastic compaction.

To determine the *EOS*, contact detonation experiments or flyer-plate impact tests can be conducted, see further Rinehart and Welch (1995), Grady (1996), and Gebbeken (2001).

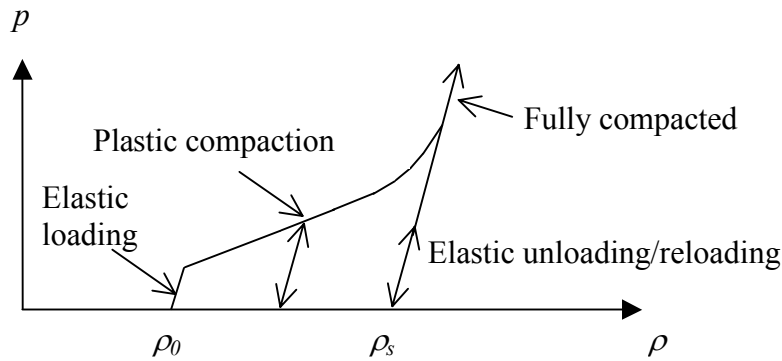


Figure 2.12 *EOS* for concrete. Based on AUTODYN (2004).

## 2.5 Strain rate effects for concrete under uniaxial loading

The strength, deformation capacity, and fracture energy are important parameters for characterizing and describing the response of concrete. For dynamic loading, these parameters are not the same as for static loading. When concrete is subjected to impact loading, the material strength becomes greater. The behaviour of concrete is determined by the loading rate; this is called the strain rate effect. The strain rate in the material depends on the type of loading, as shown in Figure 2.13 for five kinds of loading, such as creep, static, earthquake, hard impact and blast loads.

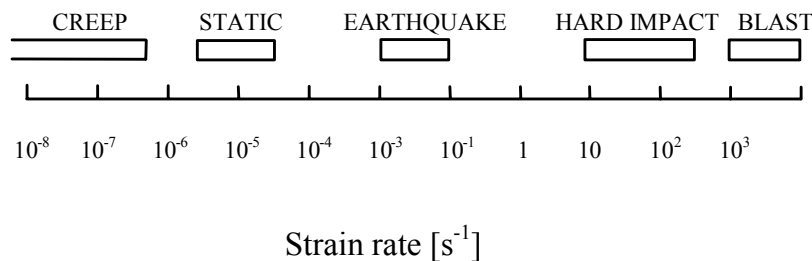


Figure 2.13 Strain rates for some types of loading; based on Bischoff and Perry (1991).

At Delft University, Zielinski (1982) followed a phenomenological approach when he compared static and impact tensions. He observed that the geometry of the fracture plane changed. With increasing loading rate, the amount of aggregate fracture became greater. Furthermore, multiple fractures were observed at high loading rates, as shown in Figure 2.14. These fracture mechanisms have a direct influence upon the stress-strain relationship for concrete in dynamic loading; the energy absorption is higher for the multiple fracture planes. Moreover, for high loading rates; the stiffness is increased, failure stress and deformation capacity are higher. In addition, the elastic stiffness is increased. This is schematically shown in Figure 2.15.

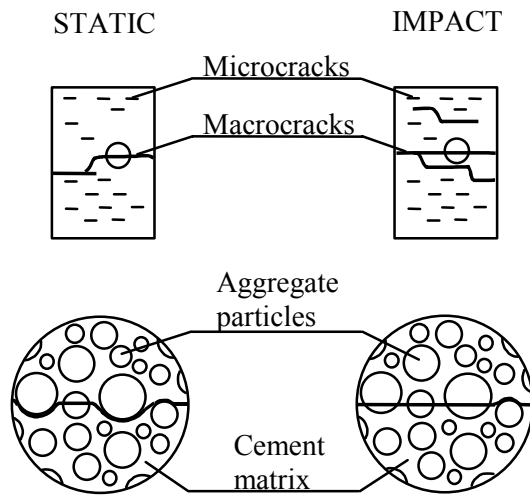


Figure 2.14 Crack path for tensile static and dynamic loading; based on Zielinski (1982).

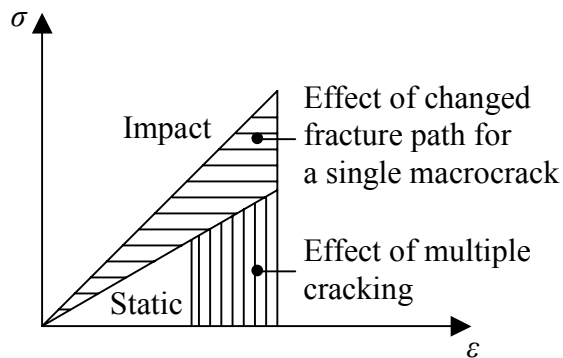


Figure 2.15 Schematic view of the effect of fracture mechanisms on the stress-strain relationship; based on Zielinski (1982).

The concrete strengths are increased by the strain rate effects. The dynamic increase factor (*DIF*) is the proportional rise of the dynamic ultimate strength relative to the static ultimate strength. The ultimate compressive strength can be more than doubled, see Bischoff and Perry (1991); experimental results are shown in Figure 2.16. Moreover, according to Ross *et al.* (1996), the concrete ultimate uniaxial strength in tension increases by multiples of 5 to 7 at very high strain rates; experimental results are shown in Figure 2.17. The greater strength is explained by the change in the fracture plane. At a higher loading rate, concrete is subject to multiple fractures, and the amount of aggregate fracture increases, see Figure 2.14. Other explanations for the increased strength are the viscous effects and the forces of inertia. This is further discussed in Paper I.

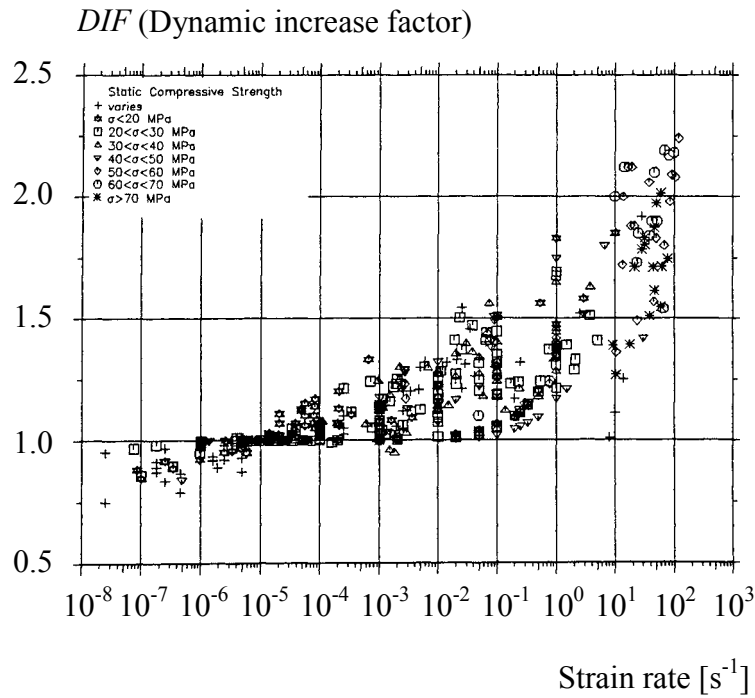


Figure 2.16 Strain rate dependency for concrete in compression; based on Bischoff and Perry (1991).

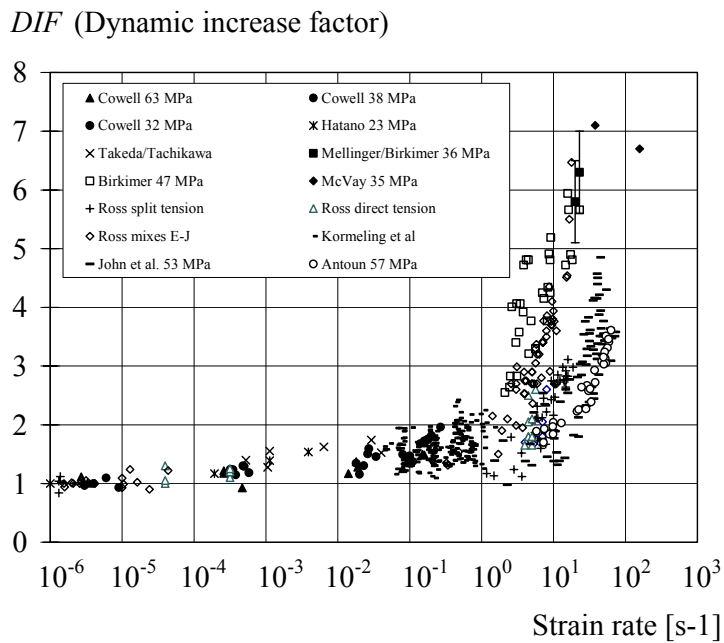


Figure 2.17 Strain rate dependency for concrete in tension; based on Malvar and Ross (1998).

## **3 Experiments on fragment impacts into concrete**

### **3.1 Introduction**

To study the concrete material properties for fragment impacts on concrete, experiments were conducted. Here a brief summary and the main results of the experiments are given; for further details, see Leppänen (2003) and Paper III. In the literature most previous experiments have been done on structural level, where beams, walls or even entire structures were analysed, see Forsén (1989), Forsén and Edin (1991), Forsén and Nordström (1992), Nordström (1992), Nordström (1993) or Nordström (1995).

Spherical fragments were shot by a detonation, in the thesis experiments, with either octol or hexotol, against thick non-reinforced concrete blocks (slightly reinforced in the edges). In a real bomb detonation, the fragments are not spherical, and the structure is reinforced. The purpose of the simplifications in the experimental set-up was to have as few uncertain parameters as possible. The depth of penetration and cratering were measured after the concrete blocks were shot. Next, to study the damage, the blocks were cut into halves so that global macro cracking could be observed. Uniaxial compressive and splitting tensile tests were made on drilled cylinders to study the change in strength. Furthermore, thin-ground specimens were prepared from the blocks, to facilitate analysis of micro-cracking with a microscope.

Another aim was to investigate how numerical methods can simulate the experiments including the loading of combined blast wave and fragment impacts; the experimental set-up was chosen in order to have clear boundary conditions for the numerical analyses. The numerical analyses are further discussed in Chapters 4 and 5 and in Paper III.

The dimensions of the blocks for the multiple fragment impacts were  $750 \times 750 \times 500 \text{ mm}^3$ , and the fragments were spherical with a radius of 4 mm. A total of seven charges were fired at an impact velocity of around 1 650 m/s. For the single fragment impacts, the dimensions of the blocks were  $750 \times 375 \times 500 \text{ mm}^3$ ; the fragments were of the same kind as for the multiple impacts. Eight single fragments were shot, however, for which the impact velocity was somewhat higher, approximately 1 850 m/s.

### **3.2 Concrete blocks that have been shot**

The concrete blocks, after being struck by fragments, were photographed as shown in Figure 3.1. The cracks were marked to improve the visualization. The depth of penetration varied between 30 and 50 mm, and the crater diameter varied between 45 and 60 mm for the concrete blocks shot with multiple fragments. To study the macro cracking in the blocks, they were cut into halves and the crack pattern was examined, see Figure 3.1 in which the crack patterns are marked. The blocks had similar overall crack patterns, with clear spalling in the impact zone; the depth of the damage zone was approximately 50 mm. At the boundaries of the blocks, a global crack pattern developed; this is caused by reflections of the stress wave generated by the impulse from the blast and fragment impacts.

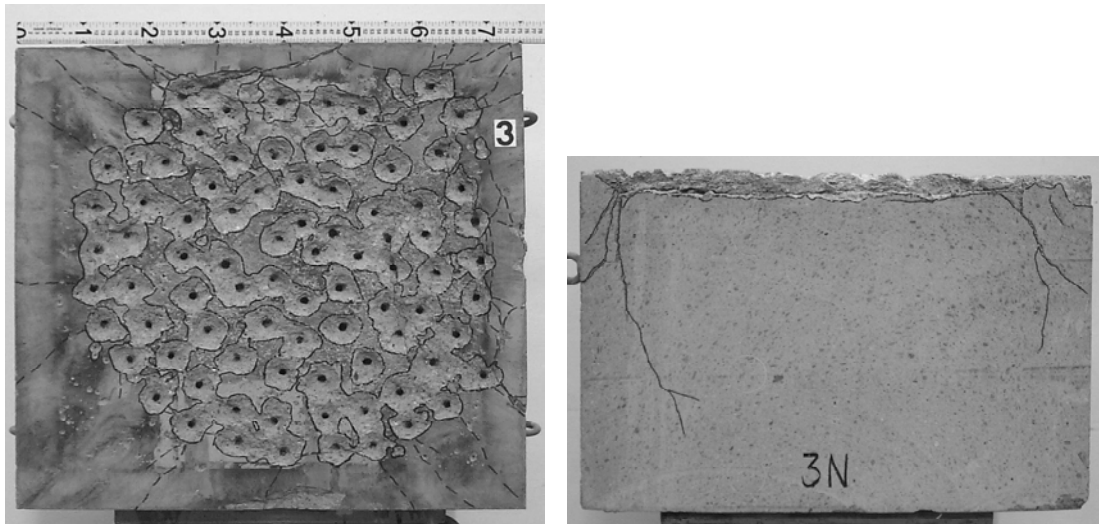


Figure 3.1 Left: Top view of concrete block No. 3 after being shot with multiple fragments. Right: Macro-crack pattern in the cross section of concrete block No. 3 (after cutting into halves).

The blocks of the single fragment impacts are shown in a photo in Figure 3.2. The average depth of penetration was approximately 55 mm, and the average crater diameter was approximately 90 mm.

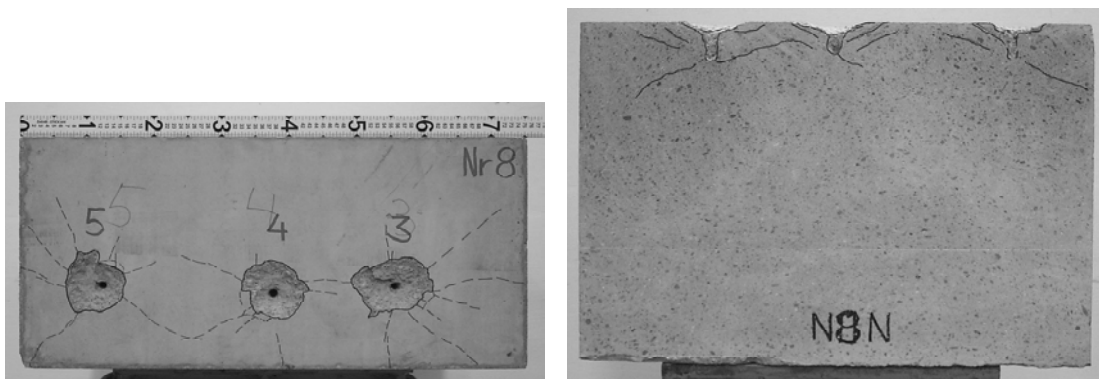


Figure 3.2 Left: Top view of concrete block No. 8 after being shot with single fragments. Right: Macro-crack pattern in the cross section of concrete block No. 8 (after cutting into halves).

### 3.3 Uniaxial compressive and tensile tests

To study the change in material properties, uniaxial compressive and splitting tensile tests were conducted on cylinders drilled from the concrete blocks. From the drilled cylinders,  $\phi 50 \times 100$  mm specimens were sawed out at various heights and smoothed for uniaxial compressive and splitting tensile tests. Cylinders were drilled in two directions: horizontally (perpendicular to the direction of the fragment impacts) and vertically. In the uniaxial compressive test on cylinders drilled in the horizontal direction, the strength was hardly affected at all by the fragment impacts, as shown in



Figure 3.3. However, for the cylinders drilled in the vertical direction, the strength was lower than for the cylinders drilled from a reference block, as shown in Figure 3.4.

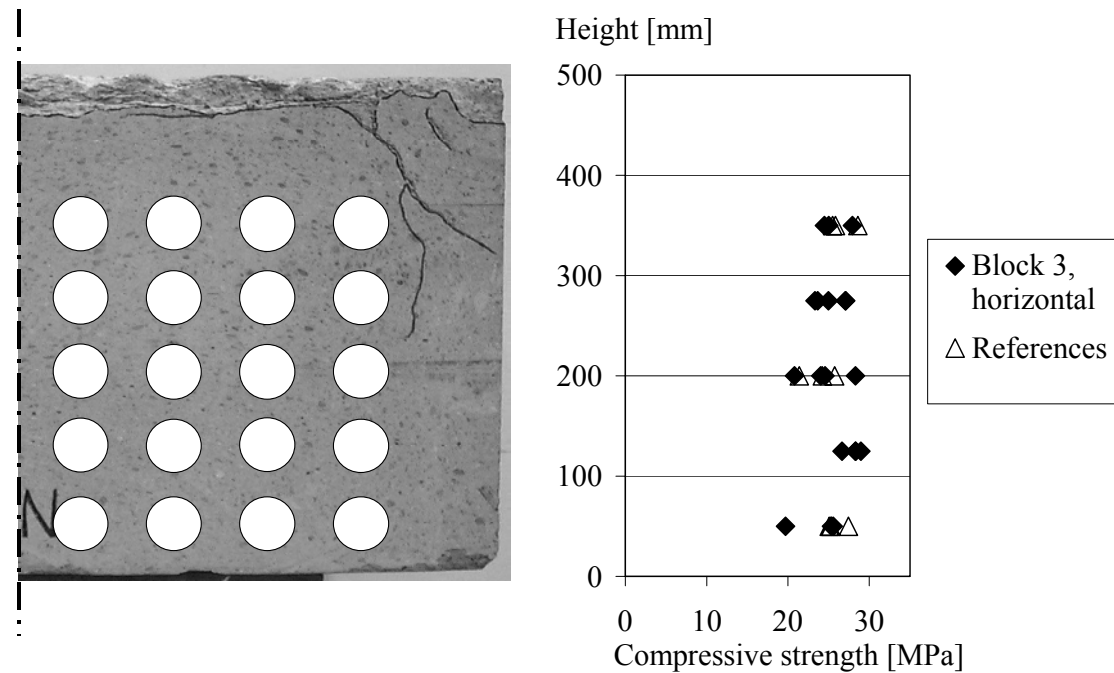


Figure 3.3 Uniaxial compressive tests on cylinders drilled horizontally from concrete block No. 3. Marked circles show where the cylinders were drilled.

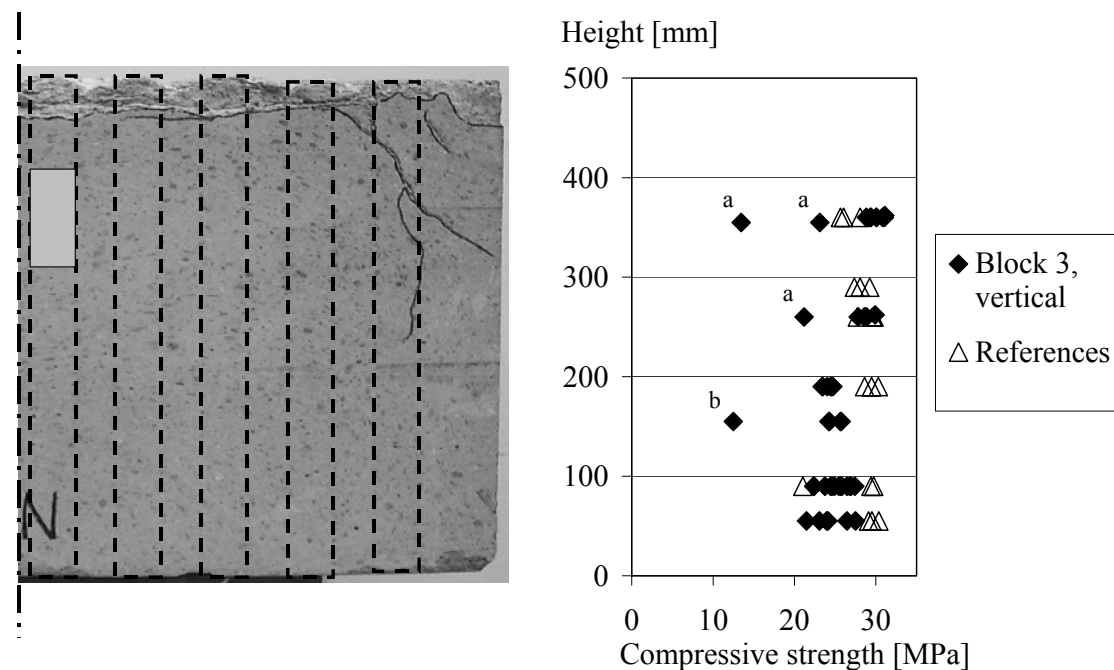


Figure 3.4 Uniaxial compressive tests for cylinders drilled vertically in concrete block No. 3. The cylinders were drilled from marked areas.

- a) The specimens were taken out near the edge
- b) A crack was visible in the specimen before the test.

Figure 3.5 shows results from the splitting tensile tests, where the cylinders were drilled vertically; the strength was hardly affected. For horizontally drilled cylinders, as for the compressive tests, the splitting tensile strength was affected very little by the blast wave and fragment impacts at a depth of 150 mm from the top surface. However, at the lower levels, where the global crack plane occurred in the cross section, the strength was reduced in most of the specimens, as shown in Figure 3.6.

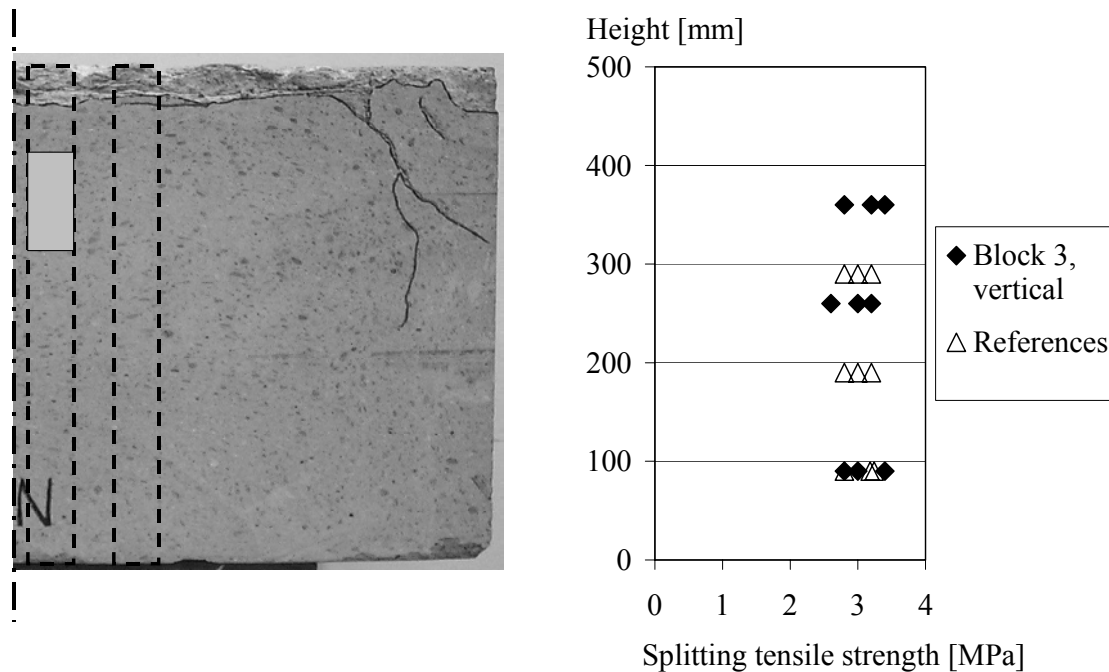


Figure 3.5 Uniaxial splitting tensile tests, vertically drilled cylinders, block No. 3.

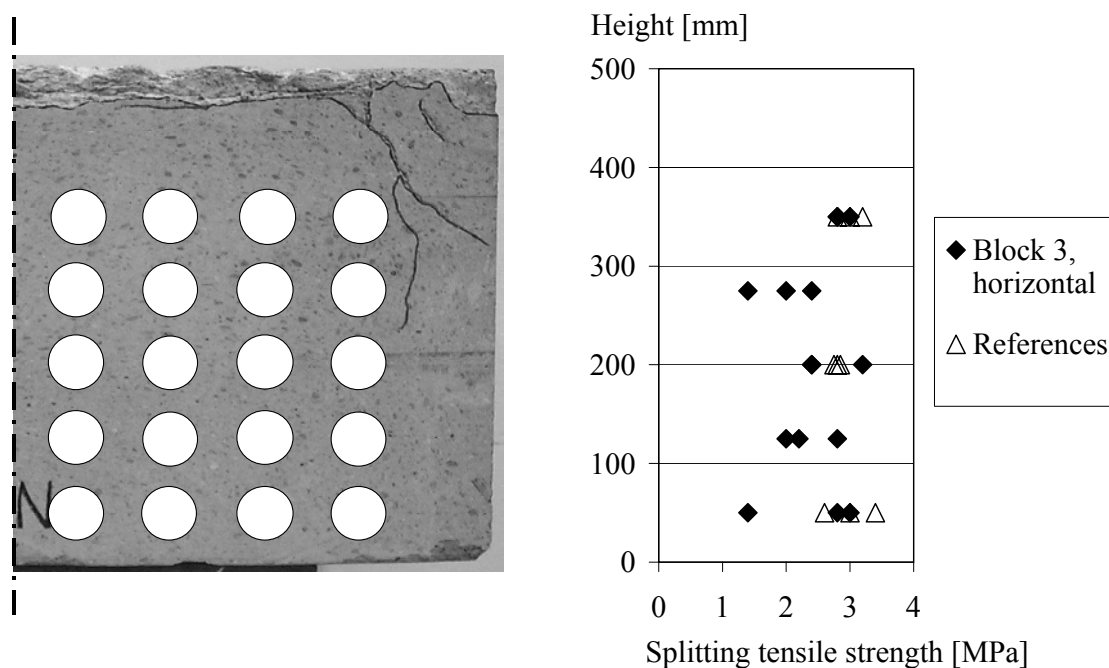


Figure 3.6 Uniaxial splitting tensile tests, horizontally drilled cylinders, block No. 3.

### 3.4 Thin-ground sections

Thin-grinding, a precise method to localize the micro-cracking in a material, is commonly used in geological studies, see Kim and McCarter (1998). To study further the micro-cracking in the concrete below the impact zone, vertically drilled cylinders from the mid sections were thin-ground to rectangular sections of 90 x 50 mm, and a thickness of 25  $\mu\text{m}$ . The sections were thin-ground from opposite sides. From the multiple fragment impact block a section was taken out at a depth between 80 and 170 mm below the surface of block No. 3. For the single fragment impact block, a section was taken out at a depth between 35 and 125 mm. As a reference, a thin-ground section was also taken from a block that was not subjected to any loading.

Photographs of the thin-ground sections were taken with a camera placed inside the microscope: examples of those with the multiple fragment impacts are shown in Figure 3.7 and with the single fragment impacts in Figure 3.8. To make the micro cracks easier to see, polarized light was used when the photographs were taken. Also before grinding, the specimens were impregnated with fluorescent penetrant, to make the cracks clearer. The thin-ground sections showed that micro cracking occurred at a depth of approximately 120 mm below the surface of the fragment impact for the multiple hits. The width of the micro cracks is up to approximately 0.02 mm.

These results verify well the uniaxial tests from drilled cylinders. The concrete strength was not affected at a depth of 150 mm; see Figures 3.5 and 3.6. For the single impacts the damage level was already reduced at a depth of approximately 75 mm. Photographs from undamaged regions were also taken and compared with photographs from a thin-ground section from the reference block as shown in Figure 3.9.

From the thin-ground sections, it can be concluded that the damage from the blast and the fragment impacts was localized at the impact zone. Micro cracking occurs at a depth of approximately twice the maximum depth of penetration of the fragments: the concrete below had no micro cracks. For the single fragment impacts micro cracking occurs to a depth of 75 mm. However, the single fragment impacts cannot be compared with the multiple fragment impacts, since the multiple fragment impacts had a blast wave added to the loading.

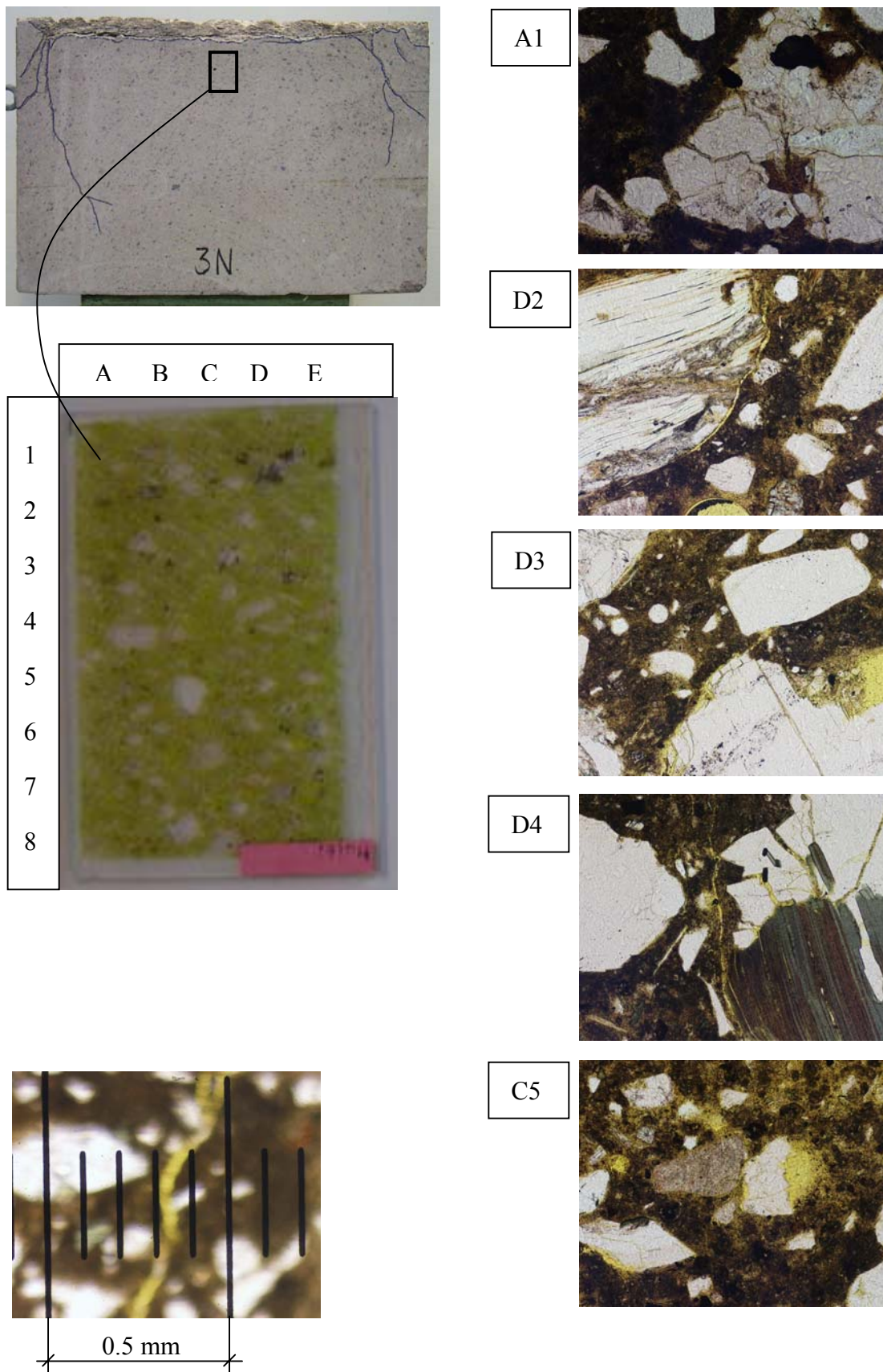


Figure 3.7 Photographs of thin-ground sections from a concrete block subjected to multiple fragment impacts.



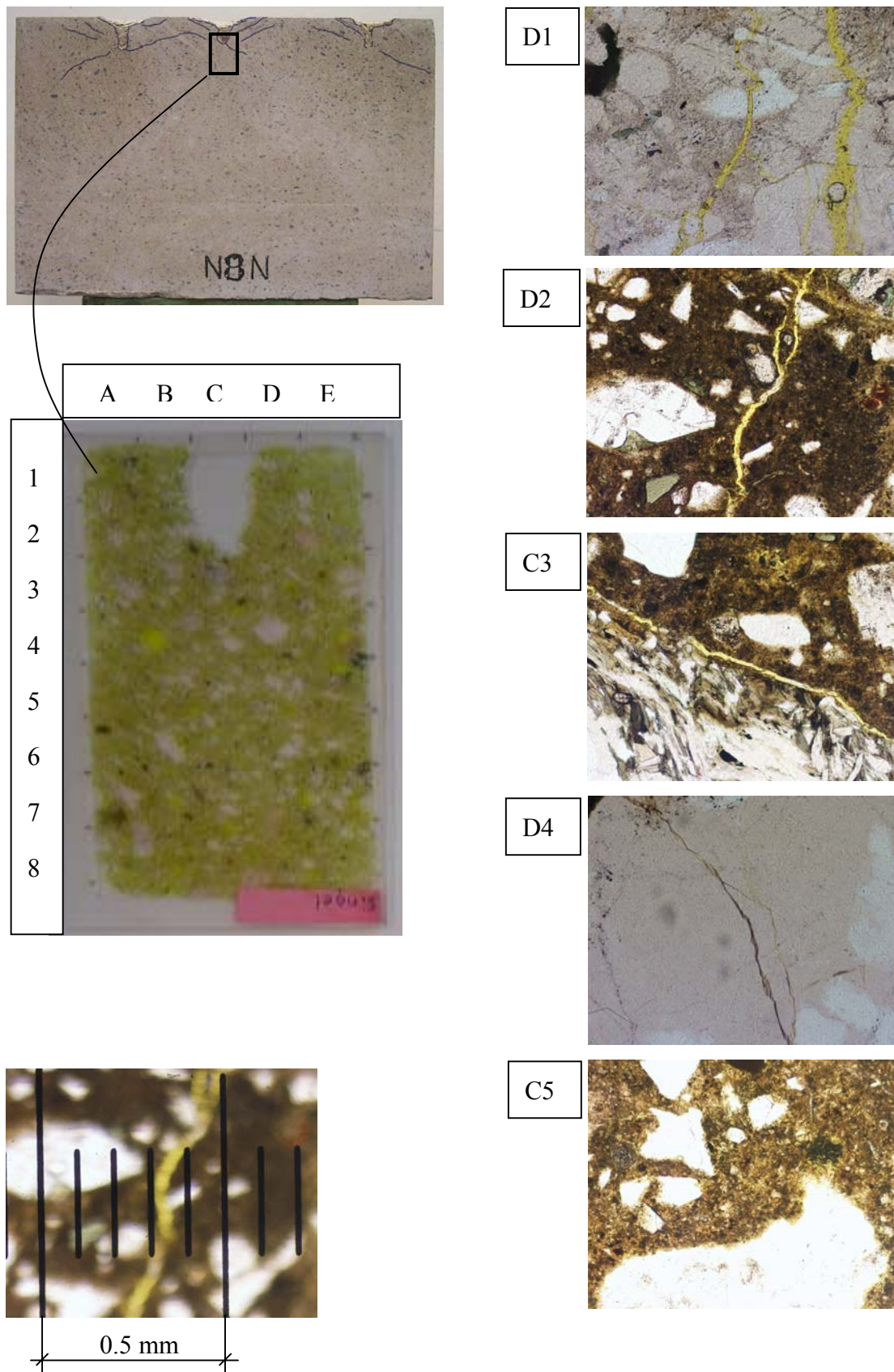
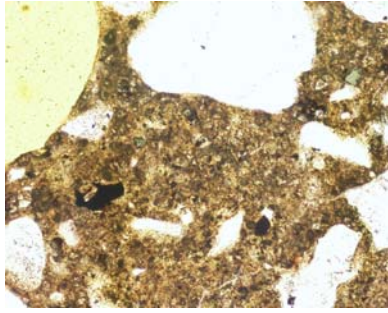
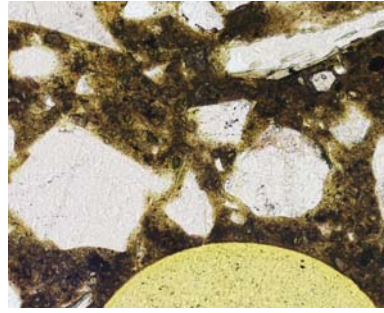


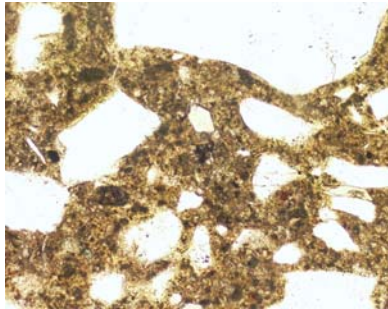
Figure 3.8 Photographs of thin-ground sections from a concrete block subjected to single fragment impacts.



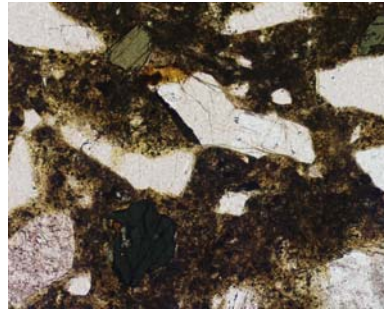
Single shot, level (C6)



Multiple shot, level (B6)



Reference



Reference

Figure 3.9 Photographs from thin-ground sections from concrete blocks subjected to single and multiple fragment impacts; and from a reference block.

## 4 NUMERICAL MODELLING

### 4.1 Numerical techniques

The development of computers in recent decades has made it possible to use numerical methods for severe dynamic loading, such as blast waves, or for penetration analyses of concrete. In the literature several papers deal with numerical analyses of projectile penetration, as in Hayhurst *et al.* (1996), Clegg *et al.* (1997), Hansson (1998), Zukas and Scheffler (2000) or Johnson *et al.* (2002). Numerical analyses of blast waves against concrete structures were carried out by Ågårdh (1997), Krauthammer (1999) and Johansson (2000). Numerical analyses of single fragment impacts were made by Bryntse (1997), Ågårdh and Laine (1999); Papados (2000) conducted numerical analyses of multiple fragment impacts.

Various numerical solvers have been used, such as the finite element method or hydrocodes. For this work the software AUTODYN (2004) was chosen. The AUTODYN program is a hydrocode, which can be used for solving a variety of problems with large deformations, and transient problems that occur for a short time, see further Benson (1992). The code combines finite difference, finite volume, and finite element techniques, see AUTODYN (2004). In hydrocodes there are multiple descriptions that can be used for the material movement, e.g. the Lagrangian, Eulerian and SPH techniques. In the Lagrangian description, the numerical mesh distorts with the material movement; in the Eulerian description, the numerical mesh is fixed in space, and the material moves in the elements, see Figure 4.1. To allow the material movement, the fixed numerical mesh is larger than the structure analysed.

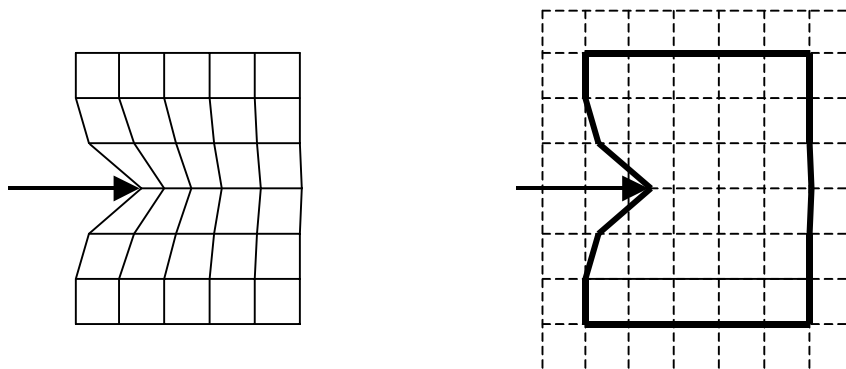


Figure 4.1 The Lagrangian description (left) and the Eulerian description (right) for material movement.

With large displacements, when using the Lagrangian description of the material movement, numerical problems arise from distortion and grid tangling of the mesh. This can lead to loss of accuracy, the time steps becoming smaller or the termination of the calculation. To overcome the numerical problems, a rezoning or erosion algorithm can be used. Rezoning transforms the numerical mesh being used into a new one. With great distortion or grid tangling, an erosion algorithm must be used to continue the calculation. Erosion is defined as the removal of elements from the analysis when a predefined criterion is reached; normally this criterion is taken to be the plastic strains. With the erosion algorithm, a non-physical solution is obtained

because of mass reduction, which means that internal strain energy is removed from the system.

The advantage of Eulerian method is that no erosion algorithm is needed, since the material moves in the elements; thus physical solutions can be obtained. However, the Eulerian method is more computationally expensive.

Both the Lagrangian and Eulerian techniques are grid-based methods. The Smooth Particle Hydrodynamics (SPH) technique does not have a grid. The advantages are that the numerical problems of grid tangling are avoided, since the technique is grid-less, and modelling of fracture can be done in a more realistic way; cracks can develop in all directions and the crack path can be followed. Kernel approximation is used in the SPH technique, see Clegg *et al.* (1997), which means that a body can be generated with interpolation points that are distributed over the volume. Each point is influenced by points in its neighbourhood, which are at a predefined distance. For example, to calculate the density of point *I* in Figure 4.2, the marked area will influence the density for this point by differing weights in relation to the distance from the point, which is the weighting function.

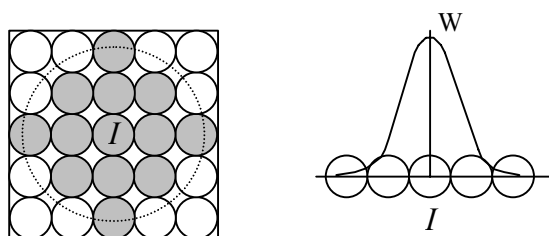


Figure 4.2 Principle of the Kernel approximation, based on Clegg *et al.* (1997). Left: a particle neighbourhood. Right: a weighting function.

The governing equations in AUTODYN are: conservation of mass, momentum and energy. To complete the description of the continuum, two additional relations describing the material behaviour are required: first the equation of state (*EOS*), and second a constitutive model.

## 4.2 The equation of state, *EOS*

The *EOS* relates the pressure to the local density (or specific volume) and the local specific internal energy of the material, according to the general equation

$$p = p(\rho, e) \quad (4.1)$$

where  $\rho$  is density and  $e$  is specific internal energy.

In finite element programs used for static analysis, a constitutive model without any explicit description of the *EOS* normally describes the material behaviour. For these programs, at high hydrostatic pressures (all principal stress components are equal), the material behaviour is linear (if the model has no cap combined with the original yield



surface). For severe loading, e.g. explosion or penetration into concrete, the hydrostatic pressure levels are so high that the non-linearity of the material behaviour must be taken into account.

The *EOS* used in the analyses carried out here is a combined P-Alpha (P stands for pressure, and Alpha is defined as the current porosity) and polynomial. In Figure 4.3 the initial density,  $\rho_0$ , is the undisturbed concrete density, and the solid density,  $\rho_s$ , is defined as the density at zero pressure of the fully compacted solid. The material behaves elastically until the initial compaction pressure,  $p_{crush}$ , is reached; thereafter, the plastic compaction phase takes place. Since no three-axial material tests were included in this project, the *EOS*, used in the numerical analyses in this thesis, is the one from AUTODYN standard library.

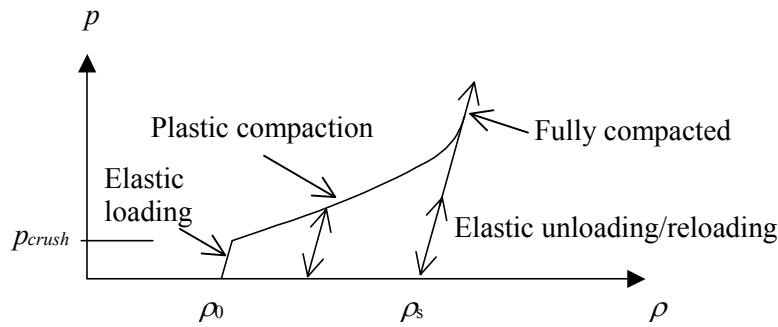


Figure 4.3 The *EOS* for concrete, combined P-Alpha and polynomial; based on AUTODYN (2004).

For hydrostatic pressure, steel compression is approximately proportional to the pressure level. Hence, a linear *EOS* for steel (fragments and projectiles) is used. The pressure level depends on the bulk modulus,  $K$ , and the compression,  $\mu$ , as shown in Figure 4.4.

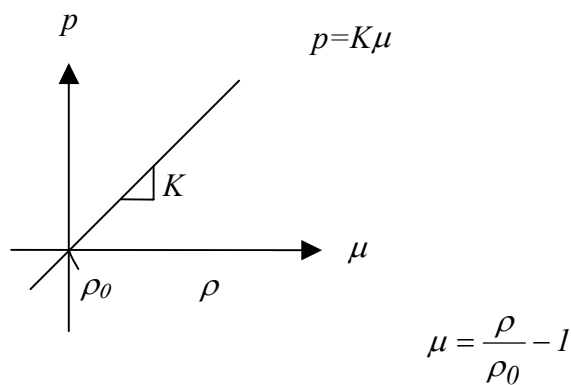


Figure 4.4 The *EOS* for steel; based on AUTODYN (2004).

### 4.3 The RHT model for concrete

The constitutive model used in the analyses with AUTODYN is the RHT model (Riedel, Hiermaier and Thoma), developed by Riedel (2000), as shown in Figure 4.5. Here, a short summary of the model is given: for detailed description of the material model, see Riedel (2000) and AUTODYN (2004). The model includes pressure hardening, strain hardening and strain rate hardening. Furthermore, the deviatoric section of the surfaces depends on the third-invariant. A damage model is included for strain softening. The model consists of three pressure-dependent surfaces: an elastic limit surface, a failure surface, and a surface for residual strength. The elastic limit surface limits the elastic stresses, and the hardening is linear up to the peak load.

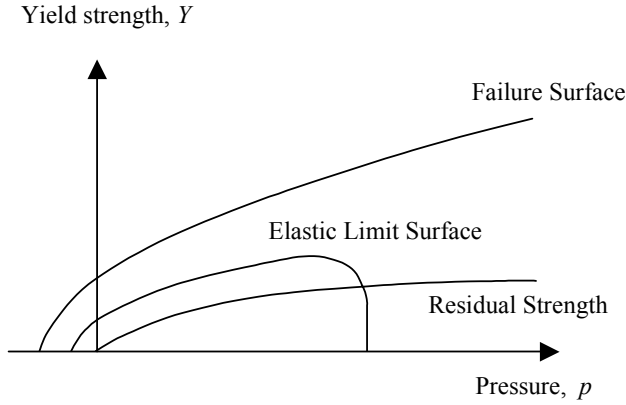


Figure 4.5 The RHT model used for concrete; based on Riedel (2000).

The failure surface is defined as

$$f(p, \sigma_{eq}, \theta, \dot{\epsilon}) = \sigma_{eq} - Y_{TXC}(p) F_{CAP}(p) R_3(\theta) F_{RATE}(\dot{\epsilon}). \quad (4.2)$$

The pressure dependency is defined as

$$Y_{TXC} = f_c \left[ A (p^* - p^*_{spall} F_{RATE})^N \right] \quad (4.3)$$

where  $A$  and  $N$  define the form of the failure surface as a function of pressure,  $p^*$  is the pressure normalized by  $f_c$ , and  $p^*_{spall}$  is defined as  $p^*(f_t/f_c)$ . The failure surface is a function of the pressure and the strain rate. The third-invariant dependence is included in the failure surface with a function,  $R_3(\theta)$ , which defines the transfer from the compressive meridian to the tensile meridian and the stress states between these.

Several expressions for the pressure dependent yield surface have been proposed, as in Ansari and Li (1998). However, the one proposed by Attard and Setunge (1996) was used in this thesis, see Figure 4.6. The failure surface (static and compressive meridian), is determined by two parameters,  $A$  and  $N$ , the values for these can be found in Appendix C. As shown in the figure, the failure surface also fits to experimental data for high confinement pressure: data from Bažant *et al.* (1996).

Figure 4.7 shows the failure surface for low pressures. The uniaxial compressive, tensile strengths and data from Attard and Setunge (1996) are shown as well.

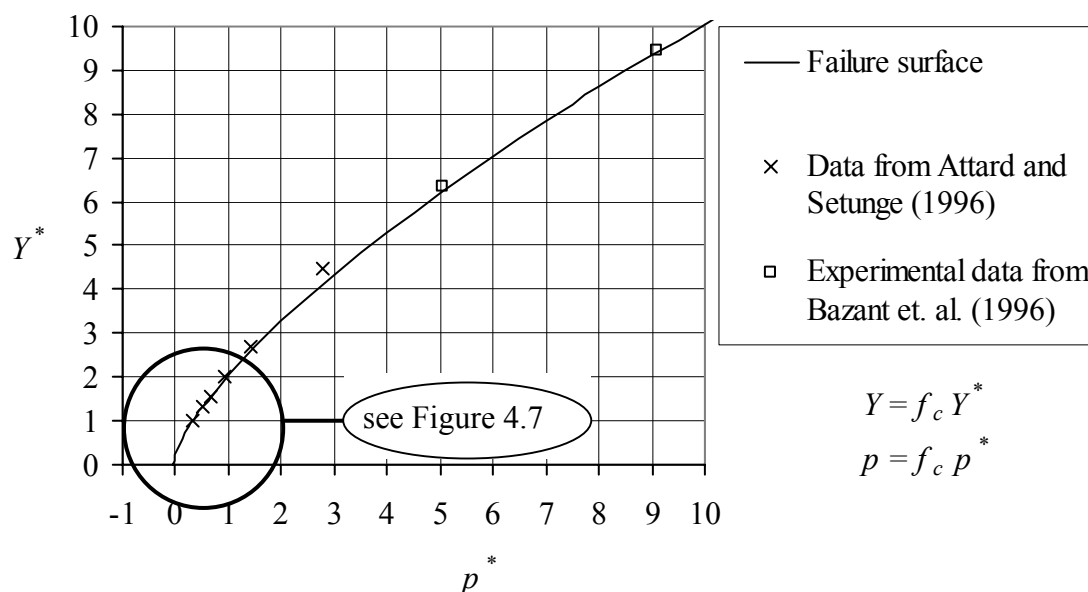


Figure 4.6 Failure surface (static, and compressive meridian);  $Y^*$  and  $p^*$  are normalized by  $f_c$ .

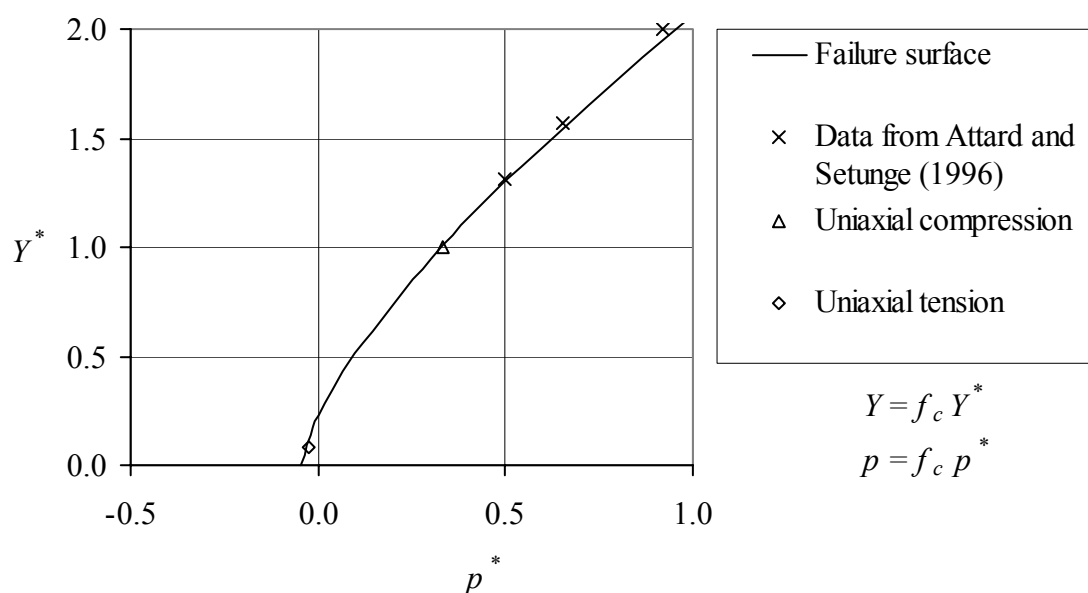


Figure 4.7 Failure surface (static, and compressive meridian) for low pressures;  $Y^*$  and  $p^*$  are normalized by  $f_c$ .

Furthermore, the RHT model has a function,  $F_{CAP(p)}$ , which limits the elastic deviatoric stresses under hydrostatic compression. The rate dependency in the yield surface is defined as

$$F_{RATE} = \left\{ \begin{array}{l} \left( \frac{\dot{\epsilon}}{\dot{\epsilon}_0} \right)^\alpha \text{ for } p > 1/3 f_c \text{ (compression), } \dot{\epsilon}_0 = 30 \cdot 10^{-6} \text{ s}^{-1} \\ \left( \frac{\dot{\epsilon}}{\dot{\epsilon}_0} \right)^\delta \text{ for } p < 1/3 f_t \text{ (tension), } \dot{\epsilon}_0 = 3 \cdot 10^{-6} \text{ s}^{-1} \end{array} \right\} \quad (4.4)$$

where  $\alpha$  is the strain rate factor for compression and  $\delta$  is the strain rate factor for tension.

When the failure surface is reached, the softening phase starts, and continues until the residual strength surface is reached. The residual strength is defined by parameters  $B$  and  $M$ , and is a function of the pressure level:

$$Y^*_{residual} = B \cdot p^{*M}. \quad (4.5)$$

The residual strength of the concrete, as shown in Figure 4.8, is calculated on the basis of the model proposed by Attard and Setunge (1996). The experiments and model, they used are for static loading with confinement pressure varying between 1 and 20 MPa. However, for projectile and fragment impacts, the confining pressure exceeds this range. Furthermore, it is not obvious that the residual strength is equal for both static and dynamic loading. Nevertheless, the Attard and Setunge (1996) model indicates the level of the residual strength. Imran and Pantazopoulou (2001) proposed a model in which the residual strength converges against the failure surface for high confinement pressures. In the numerical analyses in Section 5 and Paper IV, a new calibration of the residual strength was made, which is higher than one in the analyses reported in Papers II and III.

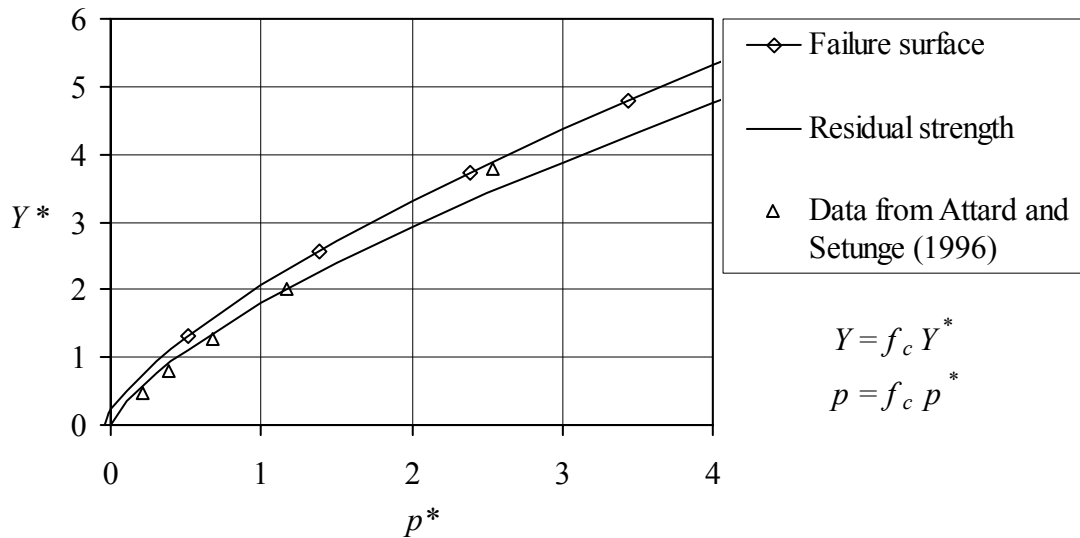


Figure 4.8 Residual strength of concrete;  $Y^*$  and  $p^*$  are normalized by  $f_c$ .

## 4.4 Mesh dependency

It is well known that the numerical mesh affects the results and that with a refined mesh the computational time increases dramatically. For dynamic loading the mesh dependency is even more sensitive than for static loading. In Johansson (2000) the mesh dependency was studied by a comparison of static and dynamic loading. He concluded that if the strain rate effect were included in the constitutive model, the general behaviour would be changed considerably. As long as the material is in the elastic stage, the strain rate is not mesh dependent. However, when the element is localised, the strain rate in the element becomes mesh dependent.

To analyse fragment impacts on concrete, a very fine mesh must be used, see Leppänen (2002) or Zukas and Scheffler (2000). The usual method is to refine the mesh and then compare the coarse mesh with the refined one, until the results differ only negligibly.

To study the mesh dependency, a prism, of length 200 mm and a cross section of 100 x 100 mm, was subjected to a tensile stress wave at one end and modelled in 3-D. The applied stress was increasing from zero to 10 MPa in 2 ms. The prism was modelled by using four quadratic meshes with element sizes of 1, 2, 5, and 10 mm, as shown in Figure 4.9. First the prism was modelled with linear elastic material properties, after which a plane corresponding to the element size was modelled as concrete, while the rest of the prism was modelled as linear elastic.

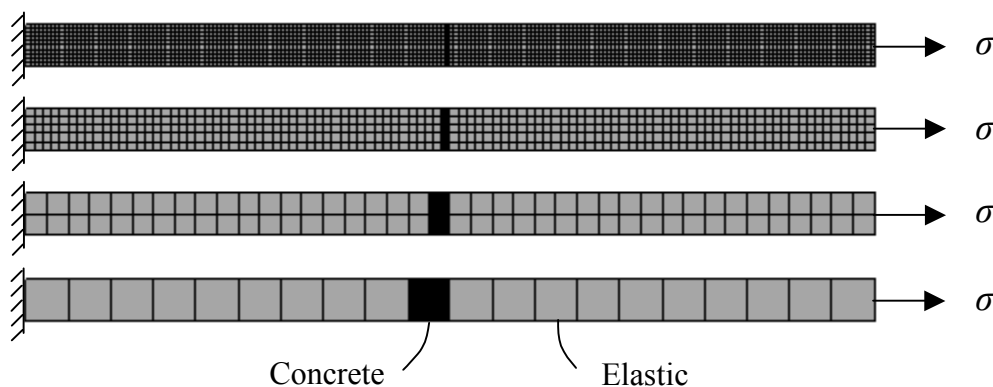


Figure 4.9 Prism subjected to a stress wave. Four meshes are compared: element sizes 1, 2, 5 and 10 mm. The marked elements are modelled as concrete, and the rest of the elements are modelled as linear elastic.

If the prism is modelled with elastic material properties for all elements, the strain rate is not mesh dependent, see Figure 4.10. However, when the concrete plane is added and the failure criterion is reached in one or several elements in the concrete, the material becomes strain rate dependent, as shown in Figure 4.11. This is due to the localisation of one or several elements in the cracked plane. Hence, the strain rate is significantly affected by the size of the mesh: the larger the mesh is, the smaller the strain rate becomes. The mesh dependency is further discussed in Section 5.

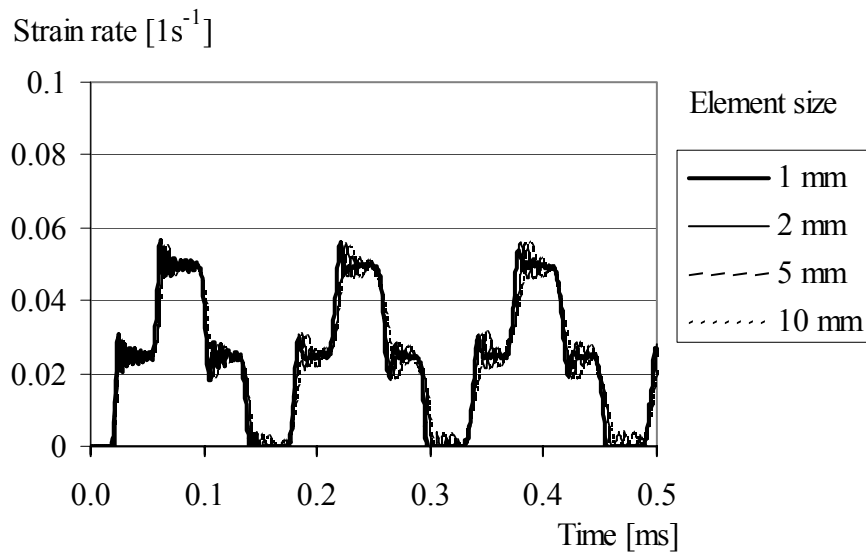


Figure 4.10 Strain rate for four meshes; elastic material behaviour.

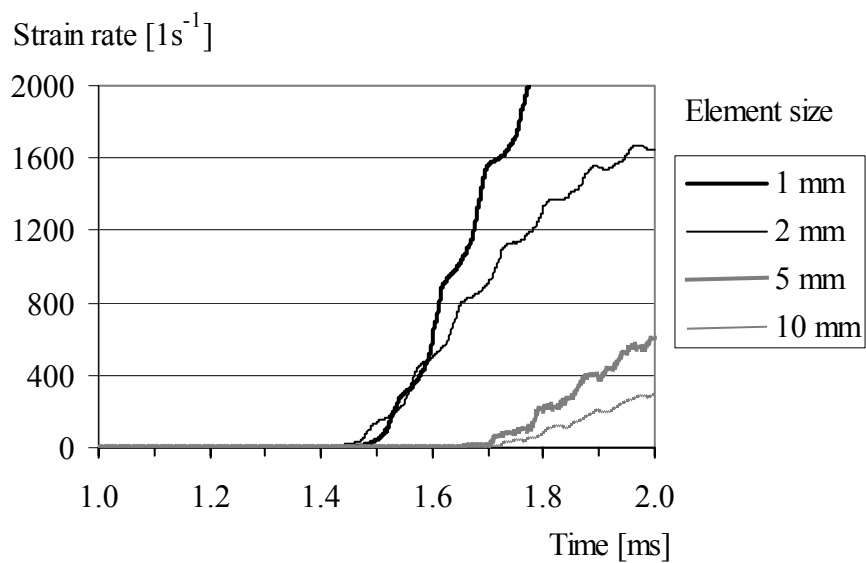


Figure 4.11 Strain rate development, after localisation, for the four meshes of different element sizes.

## 5 THE IMPROVED MATERIAL MODEL

### 5.1 General background

The RHT model in AUTODYN includes a linear softening law to model the post-failure response of concrete in tension. However, concrete is very brittle material and the strength decreases rapidly after the failure initiation. Hillerborg (1976) published a linear crack softening law for practical use of the finite element method by using fracture mechanics. The softening slope was based on the stress-crack opening relationship. The crack opening was a function of the fracture energy and the ultimate tensile strength. Later, Hillerborg introduced a stepwise-linear crack softening law to improve the accuracy of the material response, see Hillerborg (1980). Since Hillerborg presented his work, several proposals for crack softening have appeared in the literature, for example, Gylltoft (1983) and Hillerborg (1985). The formulation proposed by Gylltoft was implemented in AUTODYN, as a part of this work, and it is discussed in Section 5.2. Since, the strain rate dependency is not accurately taken into account in the RHT model, a proposal for a strain rate law by Malvar and Ross (1998) is implemented in the model used here and discussed in Section 5.3. Mesh dependency is discussed in Section 5.4, and results with the improved model are given in Section 5.5 and Paper IV.

### 5.2 The modified crack softening law

The bi-linear softening law proposed by Gylltoft (1983) was implemented in the RHT model. The softening law is based on the stress-crack opening relationship. To calculate the crack width,  $w_u$ , when the stress has fallen to zero and a real crack has formed, the fracture energy,  $G_F$ , and the tensile strength,  $f_t$ , of concrete are used, as shown in Figure 5.1. However, AUTODYN follows a smeared crack approach, and consequently the stress-strain relation is used; the maximum cracking strain is calculated from the maximum crack opening. The crack width is smeared out to a distance,  $l$ . In two-dimensional models for un-reinforced concrete, this distance is normally approximated by the square root of the area of the element, see Johansson (2000). For three-dimensional models, the length is taken to be the third root of the volume of the element. The maximum cracking strain is:

$$\varepsilon_u = \frac{w_u}{l} = \frac{4G_F}{f_t l} \quad (5.1)$$

The two slopes,  $k_1$  and  $k_2$  in Figure 5.1 for the bi-linear softening are:

$$k_1 = \frac{f_t^2}{G_F} \quad \text{and} \quad k_2 = \frac{f_t^2}{10 \cdot G_F}. \quad (5.2)$$

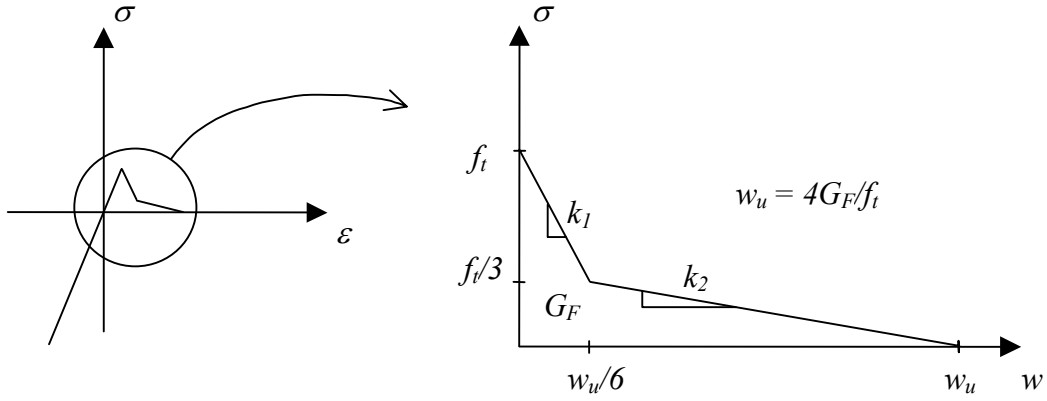


Figure 5.1 The bi-linear uniaxial stress-crack opening relationship; based on Gylltoft (1983).

For linear crack softening slope in the RHT model is

$$k = \frac{f_t^2}{2 \cdot G_F}. \quad (5.3)$$

When the tensile failure stress has been reached, the slopes in Eqs. (5.2),  $k_1$  and  $k_2$ , can be described by using the slope in Eq. (5.3) as:

$$k_1 = 2 \cdot k \quad \text{for} \quad \varepsilon \leq \frac{1}{6} \varepsilon_u \quad (5.4)$$

$$k_2 = \frac{2}{10} \cdot k \quad \text{for} \quad \varepsilon > \frac{1}{6} \varepsilon_u \quad (5.5)$$

where  $\varepsilon$  is the cracking strain and  $\varepsilon_u$  is the ultimate cracking strain (when the stress has fallen to zero).

### 5.3 The modified strain rate law for concrete in tension

Concrete is very strain rate sensitive, as described in Section 2.5. In the CEB-FIB Model Code 1990 (1993), there is a relationship for the *DIF* (dynamic increase factor) of tension as a function of strain rate. The *DIF* in the CEB is a design value, which means that the increase in strength is given at a higher strain rate than the one shown in experiments, i.e.  $30 \text{ s}^{-1}$ . However, results presented in Malvar and Ross (1998) show that the sudden increase in the *DIF* for concrete in tension occurs at a strain rate of approximately  $1 \text{ s}^{-1}$ . Figure 5.2 compares a model proposed by Malvar and Ross and the CEB. The model proposed by Malvar and Ross fits the experimental data, as shown in the figure. The equations used can be found in Appendix C.



*DIF* (Dynamic increase factor)

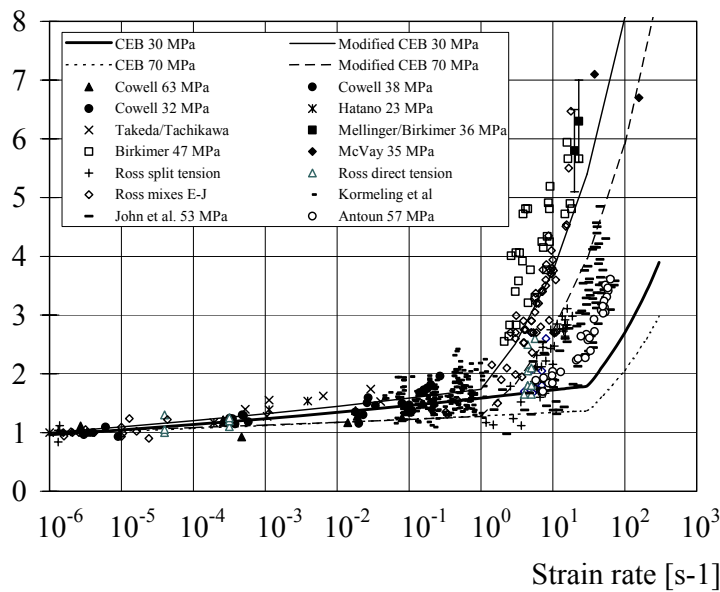


Figure 5.2 The strain rate dependency for concrete in tension. Comparison with experimental data and modified CEB model by Malvar and Ross; recommendations according to the CEB-FIB Model Code 90. Based on Malvar and Ross (1998).

In the RHT model the *DIF* for tension is determined by the parameter  $\delta$ , see Eq. (4.4). Figure 5.3 shows the *DIF* for two values of  $\delta$ . As seen in the figure, this parameter cannot be chosen in a way that fits the experimental data in Figure 5.2. For this reason a strain rate law was implemented in the RHT model. The strain rate law was implemented as stepwise linear, which means any *DIF* relationship can be chosen by the user; in the figure the chosen *DIF* according to Malvar and Ross (1998) is shown.

Moreover, Weerheijm (1992) reported that the fracture energy was of the same value for static and dynamic loading. Thus, the fracture energy in the modified RHT model is assumed to be constant. A constant value for the fracture energy in combination with higher strength, due to the strain rate effect, causes the ultimate cracking strain to decrease. Hence, the material behaviour becomes more brittle at higher strain rates for a single crack. However, in impact loading several cracks develop simultaneously; consequently the absorbed energy increases, see Svahn (2003). An example of static and dynamic stress-strain relationships is shown in Figure 5.4.

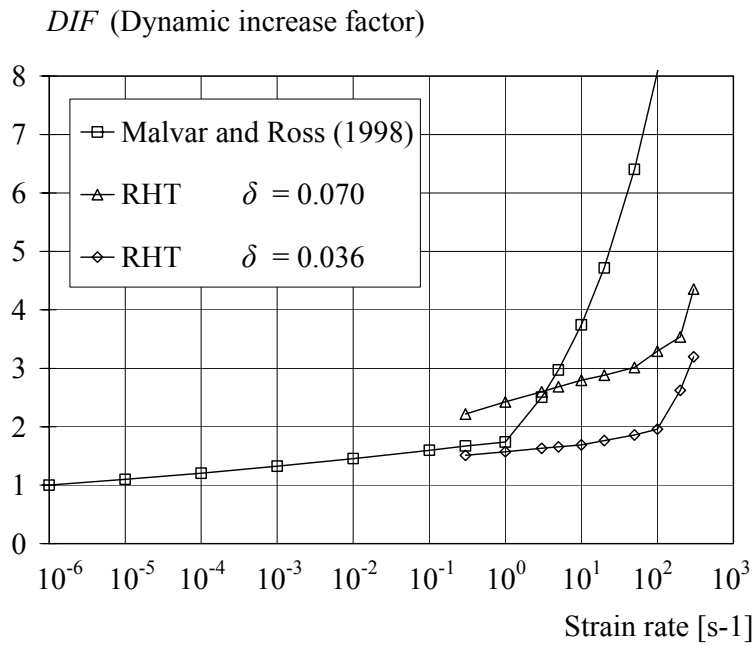


Figure 5.3 The strain rate dependency for concrete in tension with the RHT model and the modified strain rate law.

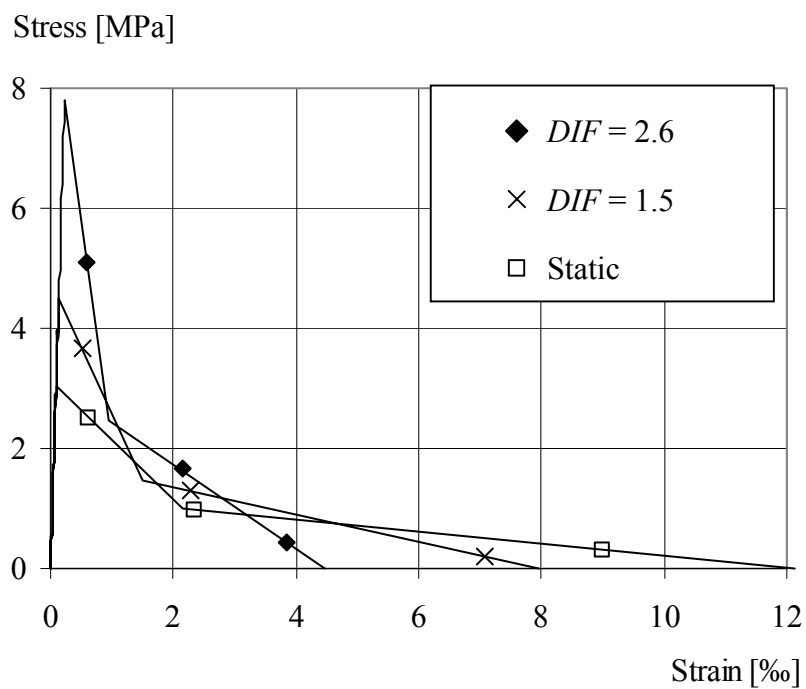


Figure 5.4 The stress-strain relationship for three strain rates. The fracture energy,  $G_F$ , is constant, therefore, the ultimate strain,  $\epsilon_u$ , decreases with an increasing strain rate.

## 5.4 Mesh dependency

Localisation of an element in a mesh leads to the material becoming strain rate dependent. The localisation has a large effect on the strain rate, and consequently on the *DIF*. Therefore, the tensile failure stress can increase after the localisation of one or several elements, as shown in Figure 5.5; this behaviour is not realistic.

For this reason, to overcome the mesh dependency problem, a cut-off is included in the modified material model. The cut-off limits the tensile failure stress; the value is determined while the material is still in the elastic stage. The stress value chosen starts from the time step when static tensile strength is reached. From this time step the *DIF* is calculated from the actual strain rate, and the failure stress is then determined from the *DIF*. Figure 5.6 shows the tensile failure stress for the four meshes tested in Section 4.4; it is shown that, when using the cut-off, the failure stress becomes approximately the same independent of the element size. Figure 5.6 also shows the stress-time history for these four meshes. For this example the static tensile strength is equal to 5 MPa. In the subroutine in AUTODYN, the failure stress is determined when the static tensile strength has been reached: for this example approximately at 1.0 ms. If the tensile stress is below the static tensile strength, the failure stress has a value of zero. At the point when the tensile stress has reached, the value of the failure stress, the softening starts.

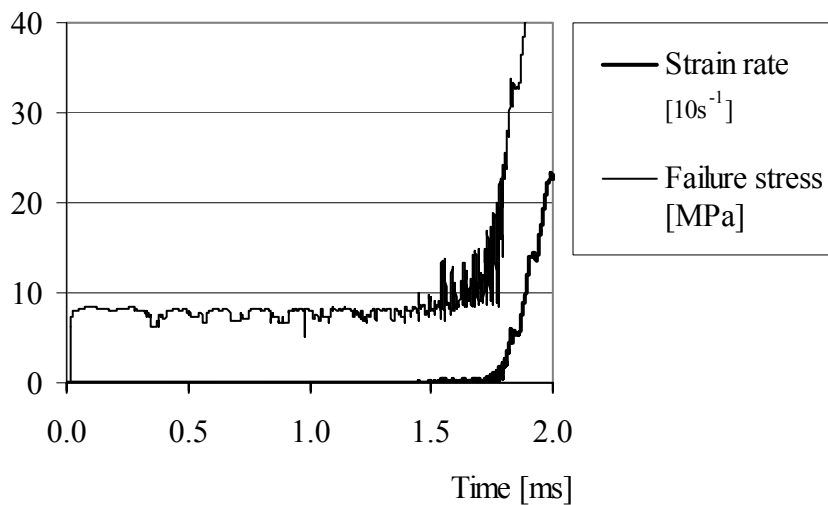


Figure 5.5 The crack softening failure stress and strain rate development after localisation.

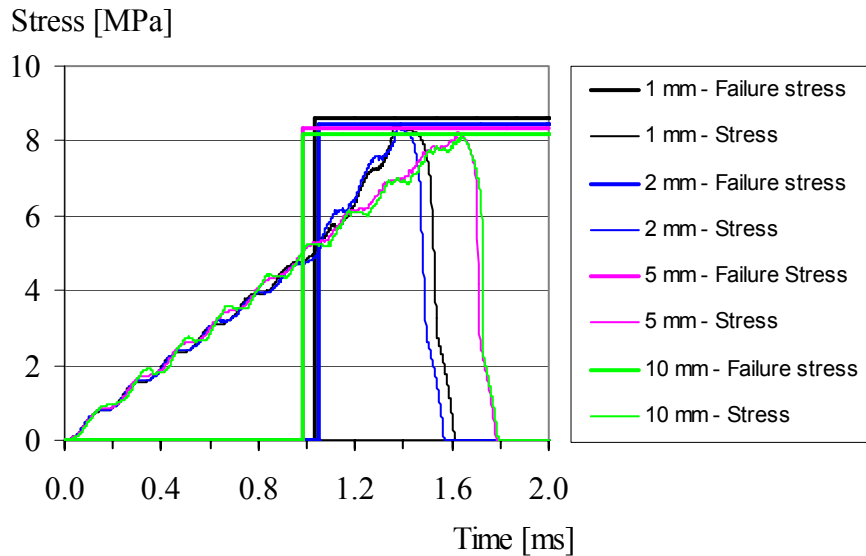


Figure 5.6 The failure stress and axial stress in the loading direction for the four meshes.

Zukas and Scheffler (2000) studied projectile impacts on concrete, and concluded that, for accuracy, there should be at least three elements across the radius of the projectile. Numerical analyses in this thesis were made for fragment impacts, with four meshes, see Table 5.1. In the analyses a spherical fragment with a radius of 10.3 mm strikes a concrete wall with a thickness of 250 mm. The fragment impact velocity was 1 201 m/s and the material parameters were the same as those in the last example in this section. Figure 5.7 shows the damage plot from the numerical analyses for the four meshes. The damage is approximately the same for element sizes 1 and 2 mm, and the depth of penetration converge for the element size of 2 mm.

Table 5.1 Mesh dependency, sizes and number of elements for the target. Crater diameter and depth of penetration.

Mesh	Size of element [mm]	Number of elements	Crater diameter [mm]	Depth of penetration [mm]
a)	4	63 x 125	130	26.6
b)	3	83 x 167	132	45.9
c)	2	125 x 250	144	86.8
d)	1	250 x 500	142	89.8

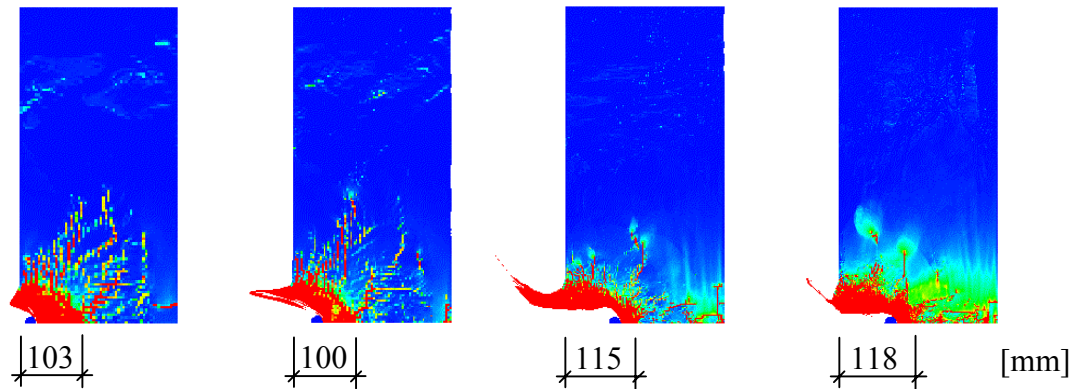


Figure 5.7 Effects of meshing on crater size. From left: mesh a, b, c and d.

## 5.5 Results with the improved material model

A reliable model must be able to describe experimental results from several different experiments with varying mass and velocities. Numerical analyses with the improved RHT model were made, and examples can be found in Paper IV. Furthermore, a parametric study was conducted (Paper IV), in which the fracture energy, tensile strength, the softening slope and the strain rate were examined. The crack width and scabbing increase with decreasing static tensile strength. By increasing the fracture energy, the cracking and scabbing were greatly reduced. Using a bi-linear softening law for tension increases the damage and the diameter of scabbing only slightly more than using a linear one. Moreover, the scabbing was greatly influenced by the choice of strain rate law. Thus, it is important to have accurate material properties to capture the concrete behaviour. The tensile strength and fracture energy used are calculated according to the CEB-FIB Model Code 1990 (1993). The bi-linear softening law proposed by Gylltoft (1983) was used, which follows the softening slope in tension more accurately than a linear one. The strain rate law used is the one proposed by Malvar and Ross (1998), which fits the experimental data well.

In a example where a single fragment perforates a concrete wall, experiments reported by Erkander and Pettersson (1985) were analysed with the Lagrangian, Eulerian and SPH techniques. The wall was 1000 x 1000 mm with a thickness of 70 mm, and the fragments were spherical with a radius of 10.3 mm and an impact velocity of 358 m/s. The concrete had an average cube strength of 35 MPa (tested on 150 mm side cubes), which corresponds to a mean value of cylinder strength of 30 MPa according to the CEB-FIB Model Code 1990 (1993). The tensile strength and fracture energy were also calculated according to the CEB; tensile strength was 2.34 MPa and fracture energy was 82.5 Nm/m<sup>2</sup>. In the experiment, the depth of penetration was 14 mm, spalling diameter was 85 mm and the diameter of scabbing was 120 mm. For the numerical analyses a 2-D axisymmetric model was used and a mesh size of 1.25 mm was chosen; consequently there were 56 x 400 elements, grids or interpolation points. The numerical analysis was in good agreement with the experiment results, especially the SPH technique, as shown in Figure 5.8.

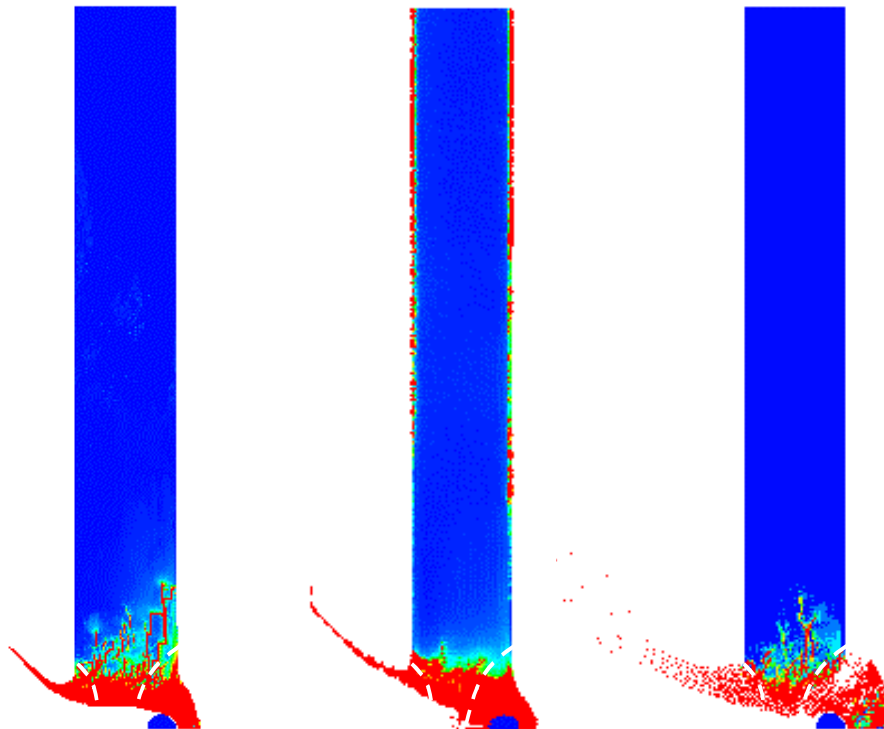


Figure 5.8 Numerical analyses with different techniques. From left: Lagrangian, Eulerian and SPH techniques. The white dashed lines show experimental results reported by Erkander and Pettersson (1985). Red area corresponds to damage equal to one, i.e. the ultimate cracking strain has been reached.

A comparison of numerical analyses with the SPH technique of fragment perforation, using the RHT model and the modified RHT model, was conducted (the same example as in Paper IV). The input data for the RHT model, and for the modified RHT model can be found in Appendix C. The spalling and depth of penetration was of the same order for both the RHT and the modified RHT models. However, the modified model improved the scabbing. The results from the numerical analyses are shown in Figure 5.9. The deviation, in scabbing diameter, between experiments and numerical analyses with the RHT model was between 6 and 28 %, while with the modified RHT model the deviation was only between 2 and 10 %.

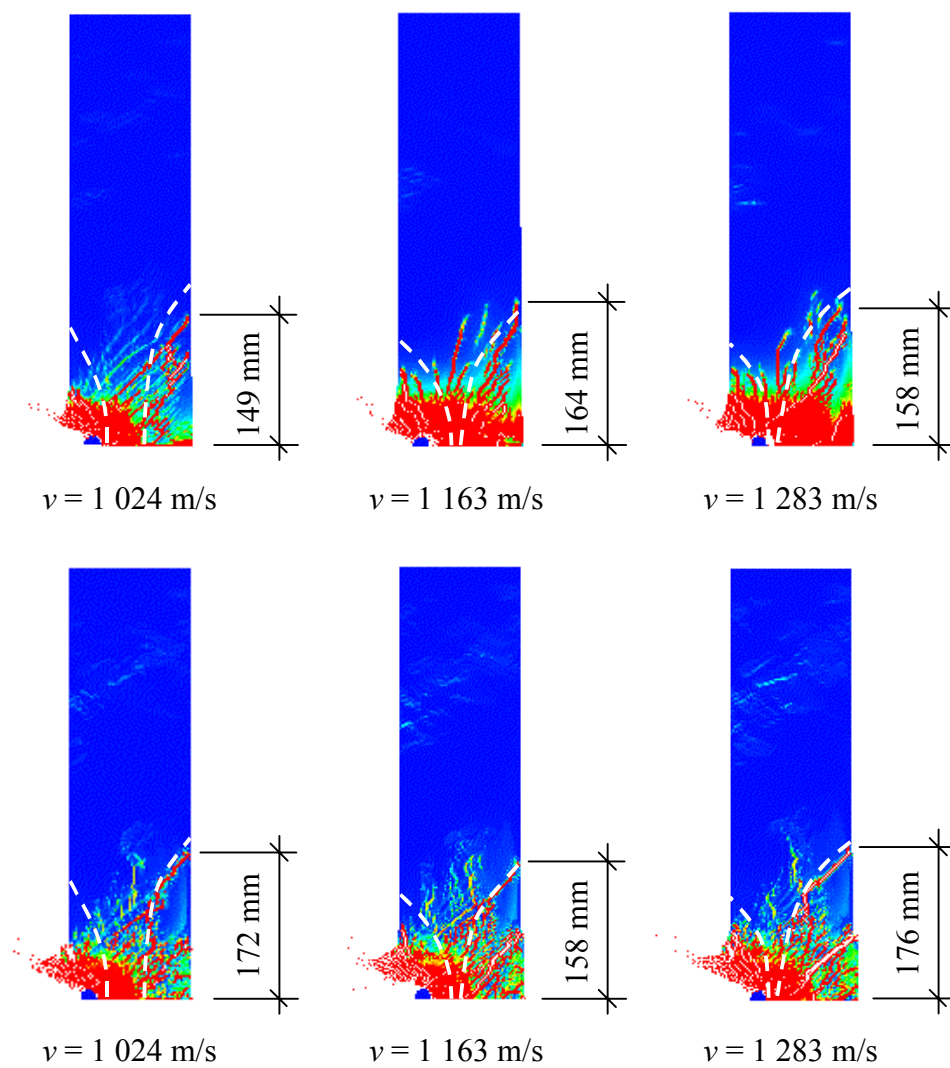


Figure 5.9 Numerical analyses of fragment penetration, concrete spalling and scabbing. White dashed lines show craters reported by Erkander and Pettersson (1985). Above: RHT model; Below: modified RHT model.

## 6 CONCLUSIONS

### 6.1 General conclusions

The aim of this thesis was to study explosive loading on civil defence shelters. The load is a combination of a blast wave and fragment impacts. However, the main focus was on the numerical modelling of projectile and fragment impacts on plain concrete members. In addition, experiments with a combination of numerical analyses were conducted to gain a deeper understanding of concrete subjected to blast and fragment impacts.

The numerical analyses carried out within the scope of this work show that this can be a very powerful tool and that fragment impacts can be modelled with advanced non-linear models. Such analyses can extend the comprehension of phenomena that cannot be revealed by conventional methods, i.e. experiments. Nevertheless, experiments are needed since they describe the reality. From previous experiments, found in the literature, empirical equations have been worked out to estimate the depth of penetration of projectiles or fragment impacts; they give quite good estimations. However, these empirical equations do not describe the material behaviour, such as cracking, failure modes or residual strength of a structure subjected to explosive loading.

Concrete structures subjected to blast and fragment impacts behave very differently from statically loaded structures. The initial stiffness and the ultimate strength, in both compression and tension, increase for dynamically loaded structures due to the strain rate effects. When a projectile or fragment hits a concrete target, the material is subjected to high strain rates, and it is also exposed to high confinement pressures. This influences greatly the depth of penetration, since the strength increases due to strain rate effects in compression, and the ultimate compressive strength increases with high pressure.

When a blast wave and fragments strike a concrete target, a compressive stress wave propagates through the concrete. When the stress wave reaches the boundaries, it will be reflected as a tensile stress wave. Since the tensile strength of the concrete is much less than the compressive strength, the reflected stress wave may cause scabbing on the side opposite the impact. The impact also causes spalling at the point of contact; the amount of spalling is influenced by the tensile strength of concrete. Furthermore, the concrete is severely cracked, and the level is influenced by the tensile strength and fracture energy of the concrete.

In the experiments thick concrete blocks were subjected to a blast wave and fragment impacts. Although both single and multiple fragments were shot, no blast wave resulted from the single fragment impacts, since these fragments were shot from a canon. In combination with the experiments, numerical analyses were made. It was concluded for the multiple impacts that the damage in the spalling zone was caused mainly by the fragment impacts. Cylinders, drilled from the shot concrete blocks, were used for uniaxial compressive and splitting tensile tests. The strength was hardly affected at a depth of approximately twice the maximum depth of penetration. Furthermore, when the blast wave was added, in the numerical analyses, there was



greater damage inside the shot concrete blocks. The increased damage was caused by reflections at the boundaries.

The software AUTODYN was used in the numerical analyses, with the Lagrangian, the Eulerian and the SPH techniques. The Lagrangian method is preferable for quick estimations. However, the SPH technique gives the most accurate results, although it is computationally more expensive.

In AUTODYN, there is a model, the RHT, to simulate concrete. The RHT model captures realistically the behaviour of concrete subjected to high pressures and high strain rates in compression. However, the model does not accurately describe concrete behaviour in tension. The softening slope in tension is modelled as linear and the strain rate law does not fit experimental results. Thus, to get an improved numerical tool for analysing projectile and fragment impacts in concrete, a bi-linear softening law was implemented in the RHT model. In addition, to capture the behaviour for concrete in tension at high strain rates, a strain rate law was also implemented. The strain rate law can be adapted to the relationship chosen for the dynamic increase factor. In the model implementation, the fracture energy chosen is constant. Moreover, the mesh becomes strain rate dependent when an element is localised (cracked element) in the numerical analyses. A cut-off that limits the crack softening failure stress was also implemented in the material model to reduce the mesh dependency.

Furthermore, a parametric study was conducted, in which the fracture energy, tensile strength, the softening slope and the strain rate were examined. The crack width and scabbing increase with decreasing static tensile strength. By increasing the fracture energy, the cracking and scabbing were greatly reduced. Using a bi-linear softening law for tension increases the damage and the diameter of scabbing only slightly more than using a linear one. It was found that the scabbing was greatly influenced by the choice of strain rate law. Thus, it is important to have accurate material properties to capture the concrete behaviour, not only for concrete in compression, also for concrete in tension. The numerical model was tested in several different experiments with projectile and fragments striking a concrete target. The accuracy of the results was better with the new model than with the existing one in AUTODYN. Hence, this model meets the need of the next generation of analysts for greater practical and deeper theoretical understanding of concrete structures subjected to blast and fragment impacts.

## **6.2 Suggestions for future research**

The work presented in this thesis is part of a research project with the long-term aim to increase knowledge of reinforced concrete structures subjected to loading with a combination of blast and fragment impacts. In the future, it is important to have a tool, which can be used for general applications and can replace expensive experiments. However, experiments can be a complement for numerical analyses.

The numerical results presented in this thesis are valid for plain concrete members. A natural continuation would be to study reinforced concrete: the interaction between concrete and reinforcement, and the effects of confinement due to the reinforcement.

The next step is structural elements, followed by whole structures. A limitation in this work is the shape of the fragments in the numerical analyses; only spherical fragments are used. To extend the work, the complexity of a whole cluster of heterogeneous fragments that fly from a bomb in combination with a blast wave can be analysed with AUTODYN.

From an explosion, besides the blast wave and fragment impacts, a lot of energy is released in the form of heat. The temperature effects were disregarded in this work. However, the time duration of the impacts is very short, and the temperature may not affect the overall response of the concrete for short-duration loads.

Finally, we need to know more about the phenomena of multi-axial dynamic loading in relation to the strain rate effects and residual strength. The material tests for residual strength are limited to static load: the question is whether the residual strength is the same for dynamic loading as for static loading.

## 7 References

- Andersson, A., Axelsson, H. and Holmström, S. (1989): *Splitter från flygbomber. Sprängningar med 250 kg mb m/50 och 500 kg mb m/56* (In Swedish). Försvarets Forskningsanstalt, FOA Rapport, C 20744-2.3, Stockholm, Sweden, January, 37 pp.
- Ansari, F. and Li, Q. B. (1998): High-strength concrete subjected to triaxial compression. *ACI Materials Journal*, Vol. 95, No. 6, Nov-Dec, pp. 747-755.
- Attard, M. M. and Setunge, S. (1996): Stress-strain relationship of confined and unconfined concrete. *ACI Materials Journal*, Vol. 93, No. 5, Sep-Oct, pp. 432-442.
- AUTODYN Manuals (2004): *AUTODYN Manuals*. Version 5, Century Dynamics, Inc., Concord, CA, USA.
- Baker, W. E. (1973): *Explosions in Air*. Univ. of Texas Press. Austin, TX, USA, 268 pp.
- Bažant, Z. P., Xiang, Y. Y., Adley, M. D., Prat, P. C. and Akers, S. A. (1996): Microplane Model for Concrete: II: Data Delocalization and Verification. *Journal of Engineering Mechanics*, Vol. 122, No. 3, March, pp. 255-262.
- Benson, D. J. (1992): Computational methods in Lagrangian and Eulerian hydrocodes. *Computer Methods in Applied Mechanics and Engineering*, Vol. 99, No. 2-3, September, pp. 235-394.
- Bischoff, P. H. and Perry, S. H. (1991): Compressive behaviour of concrete at high strain rates. *Materials and Structures*, Vol. 24, pp. 425-450.
- Bryntse, A. (1997): *Penetration av stålsplitter vid 1 500 m/s mot armerad betong (Förstudie)* (In Swedish). Försvarets Forskningsanstalt, FOA-D--97-00304-311-SE, Stockholm, Sweden, January, 9 pp.
- Bulson, P. S. (1997): *Explosive Loading of Engineering Structures*. E & FN Spon. London, UK, 233 pp.
- CEB-FIB Model Code 1990 (1993): *CEB-FIB Model Code 1990*. Design Code, Thomas Telford, Lausanne, Switzerland, 437 pp.

- Clegg, R. A., Sheridan, J., Hayhurst, C. J. and Francis, N. J. (1997): The application of SPH techniques in AUTODYN-2D to kinetic energy penetrator impacts on multi-layered soil and concrete targets. *8<sup>th</sup> International Symposium on Interaction of the Effects of Munitions with Structures*, Virginia, USA, 22-25 April, 9 pp.
- ConWep (1992): *ConWep*. Collection of conventional weapons effects calculations based on TM 5-855-1, Fundamentals of Protective Design for Conventional Weapons, U. S. Army Engineer Waterways Experiment Station, Vicksburg, VA, USA.
- Ekengren, B. (2003): *Skyddsrumregler SR* (Shelter Regulations, In Swedish). Swedish Rescue Services Agency, Publication B54-141/03, Karlstad, Sweden, 126 pp.
- Engberg, T. and Karevik, S. (1987): *Fortifikationshandbok del 1, FortH 1*. Försvarets läromedelscentral (FLC), Stockholm, Sweden, 50 pp.
- Erkander, Å. and Pettersson, L. (1985): *Betong som splitterskydd: Skjutförsök på plattor av olika betongmaterial* (Concrete as protective material against fragment impacts: Fragment impacts on concrete plates of different types of concrete, In Swedish). Försvarets Forskningsanstalt, C 20574-D6(D4), Stockholm, Sweden, May, 66 pp.
- Forsén, R. (1989): *Initialverkan, verkan på byggnader av inneslutna explosioner* (In Swedish). Försvarets Forskningsanstalt, FOA rapport C 20747-2.6, Stockholm, Sweden, February, 37 pp.
- Forsén, R. (1997): *Belastning av betongplattor med tryck och splitter från 250 kg minbomber* (In Swedish). Försvarets Forskningsanstalt, FOA-R--97-00418-311-SE, Tumba, Sweden, February, 50 pp.
- Forsén, R. and Edin, K. (1991): *Vapenverkan mot flervånings betongbyggnad III. Bestämning av skador från splitterladdningar mot husfasad i skala 1:4* (In Swedish). Försvarets Forskningsanstalt, FOA rapport C 20860-2.3, Sundbyberg, Sweden, December, 40 pp.
- Forsén, R. and Nordström, M. (1992): *Damage to Reinforced Concrete Slabs Due to the Combination of Blast and Fragment Loading* (In Swedish). National Defence Research Establishment (FOA), FOA Report B 20101-2.6, Tumba, Sweden, September, 12 pp.

- Forsén, R. and Sten, G. (1994): *Utredning om splitterverkan/splitterskydd. Jämförelse mellan två 250 kg minbomber* (In Swedish). Försvarets Forskningsanstalt, FOA dnr 94-2502/S, Sundbyberg, Sweden, April, 76 pp.
- Gebbeken, N. (2001): Determination of shock equation of state properties of concrete using full-scale experiments and flyer-plate impact tests. *Trends in computational structural mechanics*, Barcelona, Spain, pp. 109-117.
- Grady, D. (1996): Shock equation of state properties of concrete. *Structures Under Shock and Impact IV*, Udine, Italy, pp. 405-414.
- Gylltoft, K. (1983): *Fracture Mechanics Models for Fatigue in Concrete Structures*. Doctoral Thesis. Division of Structural Engineering, Luleå University of Technology, Luleå, Sweden, 210 pp.
- Hansson, H. (1998): *Numerical simulation of concrete penetration*. FOA-R, Defence Research Establishment, FOA-R--98-00816-311--SE, Tumba, Sweden, 17 pp.
- Hayhurst, C. J., Clegg, R. A., Livingstone, I. A. and Francis, N. J. (1996): The application of SPH techniques in AUTODYN-2D to ballistic impact problems. *16th International Symposium on Ballistics*, San Francisco, CA, USA, 23-28 September, 9 pp.
- Hillerborg, A. (1976): Analysis of crack formation and crack growth in concrete by means of fracture mechanics and finite elements. *Cement and Concrete Research*, Vol. 6, pp. 773-782.
- Hillerborg, A. (1980): Analysis of fracture by means of the fictitious crack model, particularly for fibre reinforced concrete. *The International Journal of Cement Composites*, Vol. 2, No. 4, November, pp. 177-184.
- Hillerborg, A. (1985): The theoretical basis of a method to determine the fracture energy  $G_F$  of concrete. *RILEM TECHICAL COMMITTEES*, Vol. 18, No. 106, pp. 291-296.
- Imran, I. and Pantazopoulou, S. J. (2001): Plasticity model for concrete under triaxial compression. *Journal of Engineering Mechanics*, Vol. 127, No. 3, March, pp. 281- 290.
- Janzon, B. (1978): *Grundläggande Stridsdelfysik* (In Swedish). Försvarets Forskningsanstalt, FOA Rapport C 20261-D4, Stockholm, Sweden, September, 164 pp.

- Johansson, M. (2000): *Structural Behaviour in Concrete Frame Corners of Civil Defence Shelters, Non-linear Finite Element Analyses and Experiments*. Doctoral Thesis. Department of Structural Engineering, Concrete Structures, Chalmers University of Technology, Publication no. 00:2, Göteborg, Sweden, 204 pp.
- Johnson, G. R., Stryk, R. A., Beissel, S. R. and Holmquist, T. J. (2002): An algorithm to automatically convert distorted finite elements into meshless particles during dynamic deformation. *International Journal of Impact Engineering*, Vol. 27, No. 10, pp. 997-1013.
- Jonasson, T. (1990): *Kontaktverkan I, Sprängladdningars kontaktverkan på armerade betongplattor* (In Swedish). Försvarets Forskningsanstalt, FOA-R, C 20809-2.6, Sundbyberg, August, 58 pp.
- Kim, D. S. and McCarter, M. K. (1998): Quantitative assessment of extrinsic damage in rock materials. *Rock Mechanics and Rock Engineering*, Vol. 31, No. 1, January - March, pp. 43-62.
- Krauthammer, T. (1999): Blast-resistant structural concrete and steel connections. *International Journal of Impact Engineering*, Vol. 22, No. 9-10, pp. 887-910.
- Krauthammer, T. (2000): *Modern Protective Structures, Design, Analysis and Evaluation*. Course notes. The Pennsylvania State University, 358 pp.
- Leppänen, J. (2002): *Dynamic Behaviour of Concrete Structures subjected to Blast and Fragment Impacts*. Licentiate Thesis. Department of Structural Engineering, Concrete Structures, Chalmers University of Technology, Publication no. 02:4, Archive no. 31, Göteborg, Sweden, 71 pp.
- Leppänen, J. (2003): *Splitterbelastad betong - Experiment och numeriska analyser* (Fragment Impacts into Concrete - Experiments and Numerical analyses, In Swedish). Department of Structural Engineering and Mechanics, Concrete Structures, Chalmers University of Technology, Report no. 03:6, Göteborg, Sweden, August, 76 pp.
- Malvar, L. J. and Ross, C. A. (1998): Review of Strain Rate Effects for Concrete in Tension. *ACI Materials Journal*, Vol. 95, No. 6, November-December, pp. 735-739.

- Nordström, M. (1992): *Splitterbelastning av betongplattor I, Metodik för bestämning av energiupptagande förmåga hos armerade betongplattor belastade med olika splittertätheter* (In Swedish). Försvarets Forskningsanstalt, FOA rapport, D 20209-2.3, Sundbyberg, October, 54 pp.
- Nordström, M. (1993): *Splitterbelastning av betongplattor II, Energiupptagande förmåga hos armerade betongplattor belastade med olika splittertätheter* (In Swedish). Försvarets Forskningsanstalt, FOA rapport, D 20226-2.3, Sundbyberg, June, 30 pp.
- Nordström, M. (1995): *Försök med experimentladdningar för simulering av splitterlast från spränggranater och minbomber* (In Swedish). Försvarets Forskningsanstalt, FOA-R--95-00109-7(6,2.6)--SE, Stockholm, Sweden, March, 54 pp.
- Nordström, M. (1995): *Splitterbelastning av betongplattor III, Energiupptagande förmåga hos armerade betongplattor belastade med olika kombinationer av splitterhastigheter, splittertätheter och splitterstorlekar* (In Swedish). Försvarets Forskningsanstalt, FOA-R--95-00094-7(6,2.6)--SE, Stockholm, Sweden, March, 101 pp.
- Papados, P. P. (2000): A reinforced concrete structure under impact: Response to high rate loads. *Sixth International Conference on Structures Under Shock and Impact*, Cambridge, UK, July, pp. 501-510.
- Plos, M. (1995): *Application of fracture mechanics to concrete bridges, Finite Element Analyses and Experiments*. Doctoral Thesis. Department of Structural Engineering, Division of Concrete Structures, Chalmers University of Technology, Göteborg, Sweden, 57 pp.
- Rempling, R. (2004): *Concrete wall subjected to fragment impacts - Numerical analyses of perforation and scabbing*. Master's Thesis. Department of Structural Engineering and Mechanics, Concrete Structures, Chalmers University of Technology, 04:1, Göteborg, Sweden, 54 pp.
- Richart, F. E., Brandtzaeg, A. and Brown, R. L. (1928): *A Study of the Failure of Concrete under Combined Compressive Stresses*. Bulletin No.185, University of Illinois, Engineering Experimental Station, Urbana, Illinois, USA.
- Riedel, W. (2000): *Beton unter dynamischen Lasten Meso- und makromechanische Modelle und ihre Parameter*. In German, Doctoral Thesis. Institut Kurzzeitdynamik, Ernst-Mach-Institut, der Bundeswehr Munchen, Freiburg, 210 pp.

- Rinehart, E. J. and Welch, C. R. (1995): Material properties testing using high explosives. *International Journal of Impact Engineering*, Vol. 17, No. 4-6, pp. 673-684.
- Ross, C. A., Jerome, D. M., Tedesco, J. W. and Hughes, M. L. (1996): Moisture and strain rate effects on concrete strength. *ACI Materials Journal*, Vol. 93, No. 3, May-June, pp. 293-300.
- Svahn, P. O. (2003): *Impact-Loaded Concrete Piles - Theoretical and experimental study of load effects and capacity*. Licentiate Thesis. Department of Structural Engineering, Concrete Structures, Chalmers University of Technology, Publication no. 02:4, Archive no. 38, Göteborg, Sweden, 51 pp.
- von Essen, W. (1973): *Provisoriska anvisningar för dimensionering av armerade betongkonstruktioner som skydd mot verkan av konventionella vapen inom närmissområde. Kommentarer* (In Swedish). Fortifikationsförvaltningen, Publ. 25:2, May, 34 pp.
- Weerheijm, J. (1992): *Concrete under impact tensile loading and lateral compression*. Doctoral Thesis. Delft University of Technology, The Netherlands, 157 pp.
- Zielinski, A. J. (1982): *Fracture of concrete and mortar under uniaxial impact tensile loading*. Doctoral Thesis. Delft University of Technology. 148 pp.
- Zukas, J. A. and Scheffler, D. R. (2000): Practical aspects of numerical simulations of dynamic events: Effects of meshing. *International Journal of Impact Engineering*, Vol. 24, No. 9, October, pp. 925-945.
- Ågårdh, L. (1997): Fe-modeling of fibre reinforced concrete slabs subjected to blast load. *Journal De Physique IV*, Vol. 7, No. C3, Aug, pp. 723-728.
- Ågårdh, L. and Laine, L. (1999): 3D FE-simulation of high-velocity fragment perforation of reinforced concrete slabs: *International Journal of Impact Engineering*, Vol. 22, No. 9, pp. 911-922.



## APPENDIX A Empirical equations

### Fragment velocity (equations used in Figure 2.6)

The initial velocity of the fragments is determined by the amount of explosive material and size of the casing, which can be estimated with an equation, where  $Q$  is the charge weight [kg] and  $M_h$  is the weight of the casing [kg], see Engberg and Karevik (1987):

$$v_i = 2400(1 - e^{-2Q/M_h}) \quad [m/s] \quad (A.1)$$

The fragment velocity is retarded in the air, depending on the initial fragment velocity, the fragment mass and the type of fragment. The retardation of the velocity after a distance,  $r$ , and for steel fragments can be calculated as, see von Essen (1973):

$$v_r = v_i e^{-0.00456r/\sqrt[3]{m_f}} \quad [m/s] \quad (A.2)$$

where  $r$  is the distance [m],  $v_i$  is the initial fragment velocity from Eq.(A.1) and  $m_f$  is the fragment mass [kg].

### Depth of penetration (equations used in Figure 2.7)

By using a direct formula, from ConWep (1992), the depth of penetration,  $x$  (in inches) can be estimated for fragments penetrating massive concrete:

$$x = \frac{0.95m_f^{0.37}V_s^{0.9}}{f_c^{0.25}} \quad \text{for } x \leq 1.4m_f^{1/3} \quad (A.3)$$

or

$$x = \frac{0.464m_f^{0.4}V_s^{1.8}}{f_c^{0.5}} + 0.487m_f^{1/3} \quad \text{for } x > 1.4m_f^{1/3} \quad (A.4)$$

where  $m_f$  is fragment weight [oz.],  $V_s$  is the fragment striking velocity [kfps] and  $f_c$  is the concrete compressive strength [ksi]. By using conversion factors, as shown in Table A.1, the penetration depth of fragments can be calculated in SI units.

The depth of penetration,  $x$ , according to von Essen (1973) can be estimated with following equation:

$$x = 180 \cdot 10^{-6} \cdot v_r \cdot \sqrt[3]{m_f} \quad [m] \quad (A.5)$$

where  $v_r$  is the fragment velocity, see Eq.(A.2), and  $m_f$  is the fragment mass [kg].

The depth of penetration,  $x$ , for a spherical fragment of 35.9 g (i.e. 20.6 mm in diameter) according to Erkander and Petterson (1985) can be estimated as:

$$x = 288 \cdot 10^{-6} \cdot \sqrt[3]{m_f} \cdot (v_r - 170) \quad [\text{m}] \quad (\text{A.6})$$

where  $v_r$  is the fragment velocity, see Eq.(A.2), and  $m_f$  is the fragment mass [kg].

### Thickness to prevent perforation (equations used in Table 2.2)

The thickness of a concrete wall that just prevents perforation,  $d_{pf}$ , can be estimated with the following equation, from Krauthammer (2000):

$$d_{pf} = 1.09xm_f^{0.033} + 0.91m_f^{0.33} \quad \text{inches} \quad (\text{A.7})$$

where  $x$  is the depth of penetration from Eqs.(A.3) and (A.4), and  $m_f$  is the fragment weight in ounce [oz]. To convert to SI units, see Table A.1.

Table A.1 Conversion factors: Inch-pound to SI units (metric), according to the ACI Manual of Concrete Practice (2002).

To convert from	to	multiply by
inches	millimeters [mm]	25.4
feet	meters [m]	0.3048
kip-force/square inch [ksi]	megapascal [MPa]	6.895
ounces [oz]	grams [g]	28.34

## APPENDIX B

### Equations to determine the dynamic increase factor

The equations to determine the *DIF* (dynamic increase factor), given by Malvar and Ross (1998) are:

$$\frac{f_t}{f_{ts}} = \left( \frac{\dot{\epsilon}}{\dot{\epsilon}_s} \right)^\delta \quad \text{for} \quad \dot{\epsilon} \leq 1 \text{ s}^{-1}$$

$$\frac{f_t}{f_{ts}} = \beta \left( \frac{\dot{\epsilon}}{\dot{\epsilon}_s} \right)^{1/3} \quad \text{for} \quad \dot{\epsilon} > 1 \text{ s}^{-1}$$

where

$f_t$  = dynamic tensile strength at  $\dot{\epsilon}$

$f_{ts}$  = static tensile strength at  $\dot{\epsilon}_s$

$f_t/f_{ts}$  = *DIF* (dynamic increase factor)

$\dot{\epsilon}$  = strain rate in the range of  $10^{-6}$  to  $160 \text{ s}^{-1}$

$\dot{\epsilon}_s$  =  $10^{-6} \text{ s}^{-1}$  (static strain rate)

$\log \beta$  =  $6 \delta - 2$

$\delta$  =  $\frac{1}{1 + \frac{8f'_c}{f'_{co}}}$

$f'_{co}$  = 10 MPa

## APPENDIX C

## Input data for the numerical model

### C.1 RHT model, equation of state (*EOS*)

Table C.1 Input data for modelling concrete: RHT model, equation of state (*EOS*).

Parameter	Value
Porous density (g/cm <sup>3</sup> )	$\rho_0^a$
Porous sound speed (m/s)	2 920
Initial compaction pressure (kPa)	$2.33 \cdot 10^4$
Solid compaction pressure (kPa)	$6 \cdot 10^6$
Compaction exponent $n$	3
Solid <i>EOS</i> :	Polynomial
Compaction curve:	Standard
$A1$ (kPa)	$3.527 \cdot 10^7$
$A2$ (kPa)	$3.958 \cdot 10^7$
$A3$ (kPa)	$9.04 \cdot 10^6$
$B0$	1.22
$B1$	1.22
$T1$ (kPa)	$3.527 \cdot 10^7$
$T2$ (kPa)	0

a. 2 400 g/cm<sup>3</sup> for the experiments with 6.28 kg projectile, Hansson (1998), 2 225 g/cm<sup>3</sup> for experiments with fragment impacts by Leppänen (2003), and 2 350 g/cm<sup>3</sup> for the experiments with fragment impacts by Erkander and Pettersson (1985).

## C.2 Constitutive model

Table C.2 Input data for modelling concrete: constitutive model.

Parameter	Value	Comments
Shear Modulus (kPa)	$G$	a
Compressive Strength $f_c$ (MPa)	$f_c$	a
Tensile Strength $f_t/f_c$	0.071 - 0.091	a
Shear Strength $f_s/f_c$	0.18	(default)
Failure Surface Parameter $A$	2	b
Failure Surface Parameter $N$	0.7	b
Tens./Compr. Meridian Ratio	0.6805	(default)
Brittle to Ductile Transition	0.0105	(default)
G(elas.)/G(elas-plas.)	2	(default)
Elastic Strength/ $f_t$	0.7	(default)
Elastic Strength/ $f_c$	0.53	(default)
Use Cap on Elastic Surface	Yes	(default)
Residual Strength Const. $B$	1.8	b, c and d
Residual Strength Exp. $M$	0.7	b
Comp. Strain Rate Exp. $\alpha$	0.032	(default)
Tens. Strain Rate Exp. $\delta$	User-subroutine	d
Max. Fracture Strength Ratio	$1 \cdot 10^{20}$	(default)
Damage constant $DI$	0.04	(default)
Min. Strain to Failure	0.01	(default)
Residual Shear Modulus Frac.	0.13	(default)
Tensile Failure model	User-subroutine	d
Erosion Strain/instantaneous geometric strain (only for Lagrange)	1.5	c

a. Material tests or calculated according to the CEB-FIB Model Code 1990 (1993).

b. Calculated with a model proposed by Attard and Setunge (1996).

c. Calibrated by parametric studies.

d. RHT model without user-subroutine,  $B = 1.5$  and  $\delta = 0.025$  were used. The tensile failure model hydro was used.

